Geomorphology 393 (2021) 107941

Contents lists available at ScienceDirect

Geomorphology

journal homepage: www.elsevier.com/locate/geomorph

Tectonic geomorphology of an active slow-moving, intrabasinal fault: The Galera Fault (Guadix-Baza Basin, central Betic Cordillera, southern Spain)

Iván Medina-Cascales [a,*], Francisco J. García-Tortosa [b], Iván Martin-Rojas [a], José Vicente Pérez-Peña [c], Pedro Alfaro [a]

[a] Departamento de Ciencias de la Tierra y del Medio Ambiente, Universidad de Alicante, 03690, San Vicente del Raspeig, Alicante, Spain
[b] Departamento de Geología, Universidad de Jaén, Campus Las Lagunillas, 23071 Jaén, Spain
[c] Departamento de Geodinámica, Universidad de Granada, Campus de Fuentenueva, 18071 Granada, Spain

ARTICLE INFO

Article history:
Received 6 February 2021
Received in revised form 2 September 2021
Accepted 2 September 2021
Available online 8 September 2021

Keywords:
Tectonic geomorphology
Morphometric analysis
Intrabasinal fault
Landscape evolution

ABSTRACT

In this work, we prove the usefulness of morphometric analyses, typically applied to basin-border faults, to define the tectonic geomorphology of a slow-moving, intrabasinal structure: the Galera Fault (Guadix-Baza Basin, southern Spain). The Galera Fault is a 30 km-long, oblique-slip fault with major left-lateral and minor vertical slip components. Through geological and structural analyses, we define for the first time the detailed surface geometry of the fault, which is characterized by features typical of left-lateral strike-slip faults. The morphometric analysis indicates that a combination of slow slip rates and the high erodibility of the juxtaposed basin infill deposits favours a rapid landscape response to fault activity that erases many landscape effects related to active tectonics. This masking is more effective on features generated by strike-slip displacement, leaving only subtle evidence, such as local stream deflections and upstream widening of catchments. In contrast, geomorphic effects related to vertical displacement are better preserved, including the control of the geometry of the main rivers and morphological differences in the drainage network between the two fault blocks. On the upthrown fault block, streams are generally shorter and steeper and have greater valley incision, leading to the development of a badland landscape. Moreover, the vertical deformation of a Middle Pleistocene glacis surface (ca. 90 m) demonstrates the important role of this slow-moving intrabasinal fault in the generation of relief in the Betic Cordillera during recent Quaternary time. Although the impact of this fault on relief building is very low in comparison with oblique-slip, basin-border faults in the mountain range, it has a key control on the Quaternary landscape evolution.

1. Introduction

Active tectonics, together with lithology, climate conditions and sea-level variations, are the main variables controlling the evolution of landscapes and drainage systems. A wide range of well-known geomorphic features develop in landforms close to active faults in response to the permanent state of disequilibrium induced by fault displacement.

In the case of oblique-slip faults, displacement generates geomorphic effects related to both the strike-slip and vertical slip components (e.g., Eusden et al., 2000; Nicol and Van Dissen, 2002; Walker et al., 2006; Chevalier et al., 2016; Yazici et al., 2018). Typical geomorphic signatures related to the strike-slip component include effects such as offset geomorphic markers, beheaded or deflected rivers, fault-parallel elongated channels, shutter ridges, or topographic gradients with associated uplift and subsidence in antidilational and dilational jogs, respectively (e.g., Wallace, 1968; Ollier, 1981; Allen et al., 1984; Sibson, 1986; Sylvester, 1988; Jackson et al., 1996; Keller and Pinter, 1996; Zhang et al., 2003; Booth-Rea et al., 2004; Walker et al., 2006; Johnson and Watt, 2012; Gürbüz et al., 2015; Zielke et al., 2015). In addition, the vertical slip component is responsible for generating geomorphic effects such as steep and high relief mountain fronts, fault scarps, fault-facing facets, and fluvial anomalies in stream profiles or in valley incision (e.g., Davis, 1903; Bull and McFadden, 1977; Keller and Pinter, 2002; Bull, 2007; Boulton and Whittaker, 2009; Burbank and Anderson, 2013).

Most of these features can be quantitatively described through morphometric analyses. A wide number of geomorphic indices have been designed to detect such anomalies and thus evaluate the tectonic activity and geomorphic impact related to active faults (e.g., Bull, 1977; Hare and Gardner, 1985; Bull and McFadden, 1977). Morphometric analyses

* Corresponding author.
E-mail addresses: ivan.medina@ua.es (I. Medina-Cascales), gtortosa@ujaen.es (F.J. García-Tortosa), ivan.martin@ua.es (I. Martin-Rojas), vperez@go.ugr.es (J.V. Pérez-Peña), pedro.alfaro@ua.es (P. Alfaro).

https://doi.org/10.1016/j.geomorph.2021.107941

are typically performed along basin-border faults (i.e., faults that juxtapose basement rocks and basin infill sedimentary rocks) with well-developed mountain fronts (e.g., Bull and McFadden, 1977; Keller and Pinter, 2002; Silva et al., 2003; Pérez-Peña et al., 2010a; Yazici et al., 2018; Ul-Hadi et al., 2013; Marliyani et al., 2016; Matoš et al., 2016; Özsayin, 2016). Nevertheless, the application of these analyses to intrabasinal faults (i.e., juxtaposed rocks from basin sedimentary infill in both fault blocks) is uncommon. Therefore, although some authors have addressed the study of intrabasinal faults from different approaches, such as structural geology and sedimentology (e.g., Mukhopadhyay et al., 1984; Schlische, 1992; Huang et al., 2016; Liu et al., 2021), their surface geomorphic expression and their role in landscape evolution has not been widely studied (e.g., García-Tortosa et al., 2008b; Crosetto et al., 2018; Patria and Putra, 2020).

Apart from the nature of the rocks juxtaposed by the faults, the geomorphic signature of active faults strongly depends on their slip rates (e.g., Duvall and Tucker, 2015; Marliyani et al., 2016). Many studies performing morphometric analyses have been conducted in relation to faults with moderate to fast slip rates, such as the San Andreas Fault (e.g., Arrowsmith and Zielke, 2009), North Anatolian Fault (e.g., Gürbüz et al., 2015), Alpine Fault (e.g., Sutherland and Norris, 1994; Barth, 2013), and Altyn Tagh Fault (Mériaux et al., 2005). In contrast, the tectonic geomorphology of slow-moving faults (≤1 mm/yr) is less well known (e.g., Silva et al., 2003; Duvall and Tucker, 2015; van der Wal et al., 2020).

This study is focused on the geomorphic expression of active oblique-slip, intrabasinal faults characterized by slow slip rates. For this aim, we analyse the tectonic geomorphology of the Galera Fault (GF). The GF is an ~30 km-long fault located in the Guadix-Baza Basin in the central Betic Cordillera (southern Spain) (García-Tortosa et al., 2007, 2008a; Sanz de Galdeano et al., 2012). This oblique-slip fault with a main strike-slip component is located in a region dominated by active WSW-ENE regional extension (e.g., Galindo-Zaldívar et al., 2015) within an active collisional orogen. The GF accommodates the WSW-ENE regional extension that dominates the central Betic Cordillera, acting as a transfer fault for the normal Baza Fault (Fig. 1) (Alfaro et al., 2021).

The GF presents a series of characteristics that make it an interesting example to study the relationship between active faulting and recent landscape evolution: i) the GF is an intrabasinal fault that juxtaposes highly erodible sedimentary basin fill deposits; ii) it is a slow-moving fault, with a horizontal slip rate of 0.5 ± 0.3 mm/yr (Alfaro et al., 2021) and vertical slip rates of 0.08–0.24 mm/yr (García-Tortosa et al., 2011); iii) the recent capture of the Guadix-Baza Basin (ca. 600–500 ka) has exposed the GF whereby otherwise it would be covered due to active sedimentation; and iv) the Guadix-Baza Basin is a semiarid region, and following its capture, it has been dominated by extensive erosion that has shaped a very young landscape influenced by the activity of the GF. Under this framework, characterized by a combination of highly erodible sediments, low tectonic activity, and semiarid climate, our aim is to prove the usefulness of morphometric analyses, typically applied to basin-border faults, to evaluate the geomorphic expression and the role of a slow-moving intrabasinal fault in landscape development. Previous studies have demonstrated that a combination of geomorphic analysis with structural characterization of active faulting is useful in elucidating the geomorphic effects produced by fault motion in areas dominated by slow faults (e.g., Jackson et al., 1996; Eusden et al., 2000; Litchfield, 2001). Hence, we perform the first detailed geological and structural characterization of the GF to discern possible relationships between fault geometry, kinematics, and geomorphology. Then, by means of GIS-based methodologies, using high-resolution digital elevation models (DEMs) as a base, we qualitatively and quantitatively analyse the landscape effects produced by fault displacement both in the topography and drainage patterns of the study area. For this purpose, we apply several geomorphic indices that allow us to detect fault-related geomorphic anomalies, such as sharp slope gradients or differences in valley incision.

2. Geological and geomorphological setting

2.1. Recent geodynamic setting

From the late Miocene to the present, the Betic Cordillera (western Mediterranean region) has been dominated by the oblique NNW-SSE convergence of the Nubian and Eurasian plates (approximately 5–6 mm/year, DeMets et al., 2010; Nocquet, 2012). In the central sector of the Betic Cordillera, this geodynamic context is responsible for regional NNW-SSE shortening (Galindo-Zaldívar et al., 1993; Herraiz et al., 2000; Sanz de Galdeano and Alfaro, 2004) in combination with orthogonal ENE-WSW extension (e.g., Gil et al., 2002; Galindo-Zaldívar et al., 2015) of approximately 2.1–3.7 mm/yr (e.g., Serpelloni et al., 2007, Pérez-Peña et al., 2010b). In the Guadix-Baza Basin, this ENE-WSW regional extension is accommodated by NNW-SSE normal faults (e.g., the Baza Fault) and SW-NE to W-E strike-slip faults (e.g., Guerra-Merchán, 1992; Galindo-Zaldívar et al., 1999; Martínez-Martínez et al., 2006; Pedrera et al., 2006, 2012; Pedrera, 2008; Alfaro et al., 2008; García-Tortosa et al., 2011; Sanz de Galdeano et al., 2012, 2020; Galindo-Zaldívar et al., 2015; Medina-Cascales et al., 2020) (Fig. 1).

The GF (Fig. 1) is one of the active SW-NE faults accommodating regional extension in the Guadix-Baza Basin (García-Tortosa et al., 2007, 2011). The GF is an oblique-slip fault that presents a main strike-slip component of displacement and a minor vertical (normal) component of displacement. The fault is characterized by slow slip rates, with a short-term horizontal slip rate of 0.5 ± 0.3 mm/yr calculated by GPS data (Alfaro et al., 2021) and a long-term vertical slip rate of 0.08–0.24 mm/yr (García-Tortosa et al., 2011). The GF is kinematically related to the normal Baza Fault (Fig.1), acting as a transfer structure that accommodates the extension of the Baza Fault to the east (Alfaro et al., 2021). The GF is responsible for several low-magnitude historical earthquakes, including the June 9th 1964 (mbLg 4.8, VIII) SW Galera earthquake (Martínez-Solares and Mezcua, 2002; García-Tortosa et al., 2007; Silva Barroso et al., 2014).

2.2. Geology and geomorphology of the Guadix-Baza Basin and Baza Subbasin

The GF extends close to the NE margin of the Guadix-Baza Basin (Fig. 1), which is the largest of the Neogene–Quaternary intramontane basins in the Betic Cordillera (Vera, 1970a, 1970b). The Guadix-Baza Basin is located at the boundary between two important domains within the Betic Cordillera that act as the basin basement: the Betic Internal Zones (Paleozoic and Mesozoic metamorphic rocks) and the Betic External Zones (mainly Mesozoic and Tertiary sedimentary rocks) (Fig. 1) (Sanz de Galdeano and Vera, 1992). The basement is covered by a sedimentary infill consisting of upper Miocene, Pliocene and Quaternary sediments (e.g., García-Aguilar and Martín, 2000; García-Aguilar and Palmqvist, 2011; Gibert et al., 2007a, 2007b; Guerra-Merchán, 1992; Peña, 1979, 1985; Soria et al., 1987; Vera, 1970a, 1970b; Vera et al., 1994; Viseras, 1991; Soria et al., 1999). From the early Pliocene to the Middle Pleistocene, the Guadix-Baza Basin was an endorheic basin (Gibert et al., 2007a, 2007b; García-Tortosa et al., 2008a, 2011), resulting in the accumulation of continental sediments (e.g., Vera, 1970a, 1970b; Peña, 1979, 1985; Viseras, 1991; Vera et al., 1994; Soria et al., 1987; Guerra-Merchán, 1992). The sedimentary environments in the basin were controlled by the extensional activity of the Baza Fault (Fig. 1), which divided the basin into two domains (Figs. 1 and 2A): the Baza sub-basin in the eastern sector (downthrown block of the BF), which was dominated by a lacustrine sedimentary environment, and the Guadix sub-basin in the western sector (uplifted block of the BF), where fluvial and alluvial sedimentary environments developed (Alfaro et al., 2008).

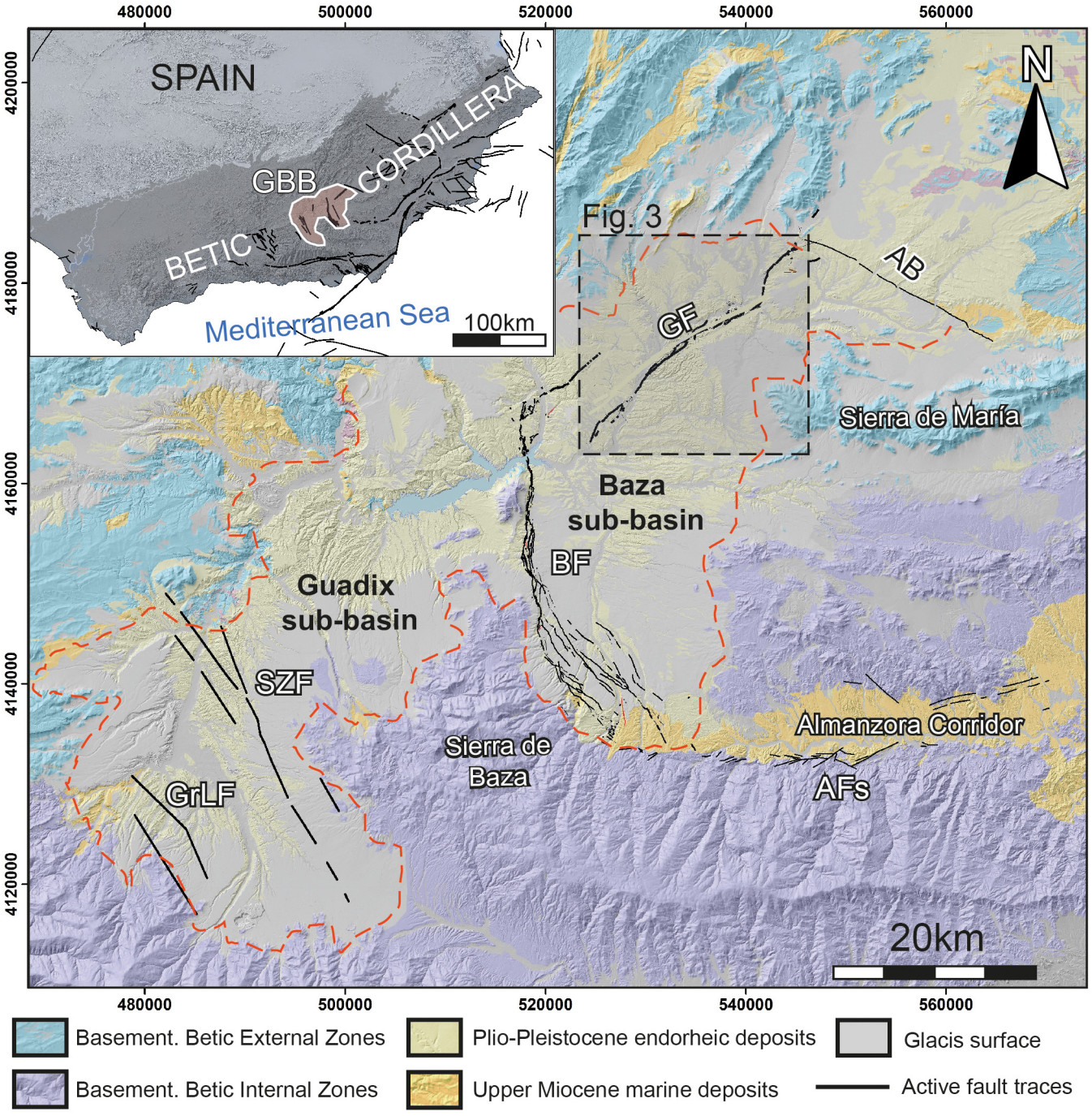

Fig. 1. Geological map of the Guadix-Baza Basin (GBB, red dashed line) and its main active structures. BF: Baza Fault, GF: Galera Fault, AFs: Almanzora Faults, AB: Alfahuara-Botardo structure, SZF: Solana de Zamborino Faults, and GrLF: Graena-Lugros Fault. The inset shows the location of the Guadix-Baza Basin in south-central Spain. DEM source: Spanish Centre of Geographical Information (CNIG, https://centrodedescargas.cnig.es/CentroDescargas/index.jsp).

The present study area (Galera Fault) is located in the Baza sub-basin (Fig. 1). During the endorheic stage of the Guadix-Baza Basin (Fig. 2A), extensive sedimentation in the Baza sub-basin resulted in a thick succession of lower Pliocene to Middle Pleistocene lacustrine deposits (Gibert et al., 2007a). This sedimentary infill is configured into lithologic zones that correspond to different palaeolake sedimentary environments (Gibert et al., 2007a).

During the Pleistocene, an extensive depositional-erosive top basin surface developed across the entire Guadix-Baza Basin, capping the final stage of basin infill (Fig. 2A). This top basin surface, henceforth referred to as "glacis" (sensu Dumas, 1969), remained active until the basin became exorheic in the Middle Pleistocene (600–500 Ka, Gibert et al., 2007b; García-Tortosa et al., 2008a, 2011), when its drainage was captured by the Guadiana Menor River and re-routed towards the Atlantic (Fig. 2B) (Calvache and Viseras, 1995; Díaz-Hernández and Juliá, 2006; Scott and Gibert, 2009; García-Tortosa et al., 2008a). Some authors have proposed that the sector where capture occurred was tectonically controlled (Calvache and Viseras, 1995, 1997; Moral and Balanyá, 2020).

Hence, from the Middle Pleistocene, the Guadix-Baza sub-basin has been dominated by erosional processes (Calvache and Viseras, 1995; García-Tortosa et al., 2008a, 2011; Pérez-Peña et al., 2009). Consequently, the glacis was progressively eroded (Fig. 2D), and a complex incised fluvial drainage network was developed across the Guadix-Baza

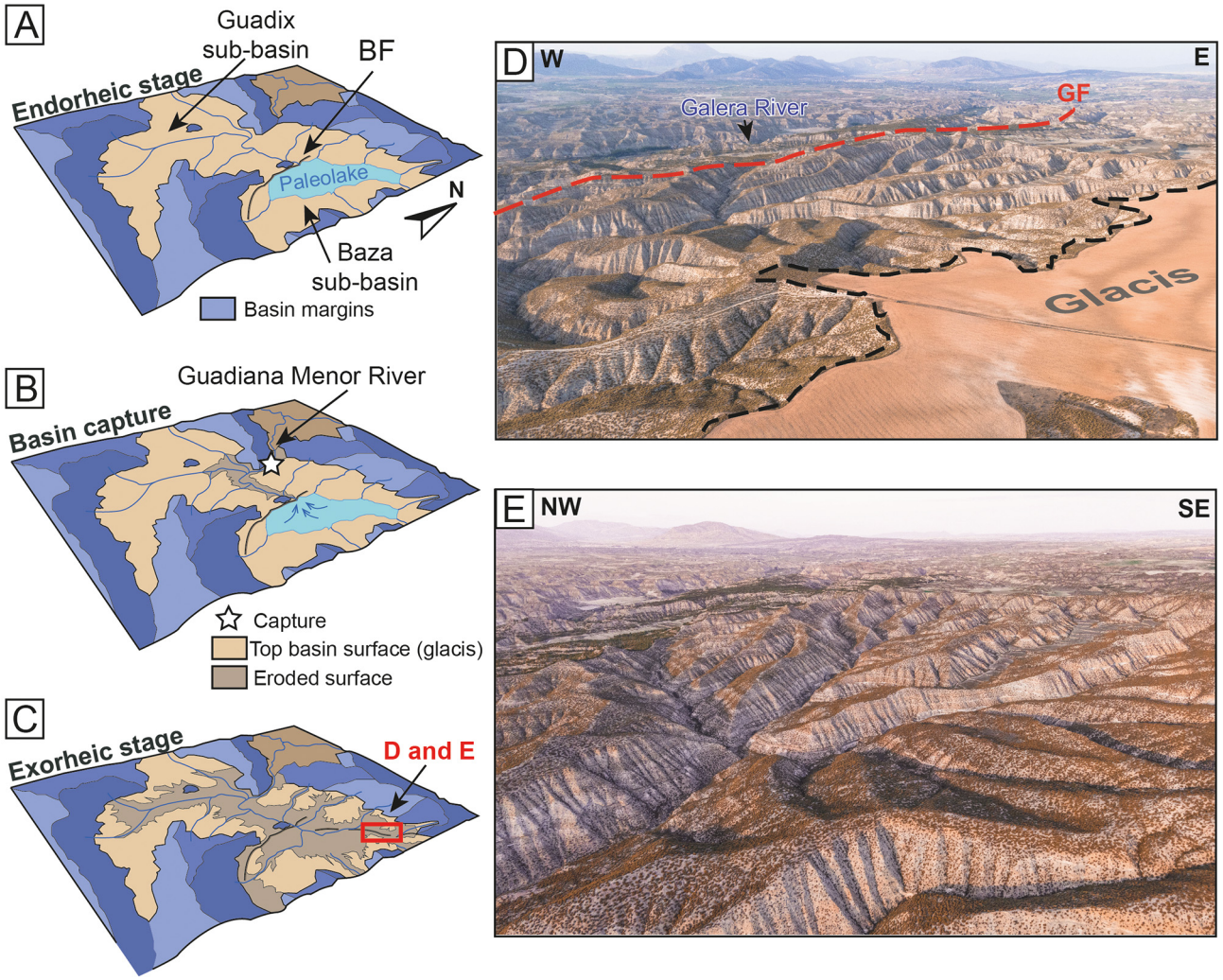

Fig. 2. Geological and geomorphological evolution of the Guadix-Baza sub-basin. (A) Endorheic stage (upper Miocene to middle Pleistocene). The Baza Fault controls the development of a fluvial environment in the Guadix Subbasin and a lacustrine environment in the Baza sub-basin. (B) Middle Pleistocene capture of the Guadix-Baza sub-basin by the Guadiana Menor River and incipient drainage network incision. (C) Exorheic stage (Middle Pleistocene to present day). Intense erosion and drainage network development that led to the (D) eroded glacis surface and development of badlands. The red dashed line represents the approximate trace of the GF. (E) Badlands landscape in the study area.

sub-basin (Fig. 2C). The post-capture base-level lowering (from ca. 1000 m to sea level), the semi-arid climate, and the high erodibility of the basin sediments resulted in intense erosion and incision by the drainage network leading to the formation of a badland landscape (Fig. 2E) that is still actively eroding today (Pérez-Peña et al., 2009; García-Tortosa et al., 2011). Since basin capture, the activity of the GF has controlled the development of the young, recent Quaternary landscape in the study area.

3. Methodology

3.1. Fault characterization

Before implementing the morphometric analysis, we first carried out geological and structural characterization of the GF. For this purpose, we conducted detailed geological mapping of the study area (1:5000 scale). The mapping is based on field observations combined with the analysis of aerial photographs and hillshade images derived from high-resolution digital elevation models (DEMs) (1 and 5 m per pixel) obtained from the Spanish Centro Nacional de Información Geográfica (CNIG, https://centrodedescargas.cnig.es/CentroDescargas/index.jsp). The geological map includes detailed geometry of the GF traces and the lithostratigraphic units cropping out in the study area. From this map, we describe the main structural features of the GF. Moreover, this geological and structural map is useful to analyse the influence of fault geometry and kinematics in the configuration of landforms (e.g., depressed areas related to transtension zones produced by strike-slip displacement) and to discriminate between tectonic and non-tectonic landscape anomalies (e.g., to observe relationships between strong slope gradients in streambeds and fault traces) (e.g., Ruszkiczay-Rüdiger et al., 2007; Ruszkiczay-Rüdiger et al., 2009). Finally, in order to measure the vertical displacement of the fault, we select a stratigraphic marker of ca. 2.3 Ma (Garcés et al., 1997). The criteria we use for selecting this marker is its lateral continuity in both fault blocks along most of the study area.

3.2. Topographic analysis

With the aim of recognizing the influence of active tectonics on the landscape, we carried out a qualitative and quantitative analysis of topographic anomalies using elevation and slope angle maps obtained from high-resolution DEMs (e.g., Zuchiewicz, 1991, 1998; Demoulin, 1998; Keller and Pinter, 2002; Ruszkiczay-Rüdiger et al., 2009; Matoš et al., 2016; García-Delgado and Velandia, 2020).

The analysis of elevation and slope maps allows us to identify potential geomorphic anomalies, such as depressed or uplifted areas related to fault geometry and displacement (e.g., García-Delgado and Velandia, 2020),

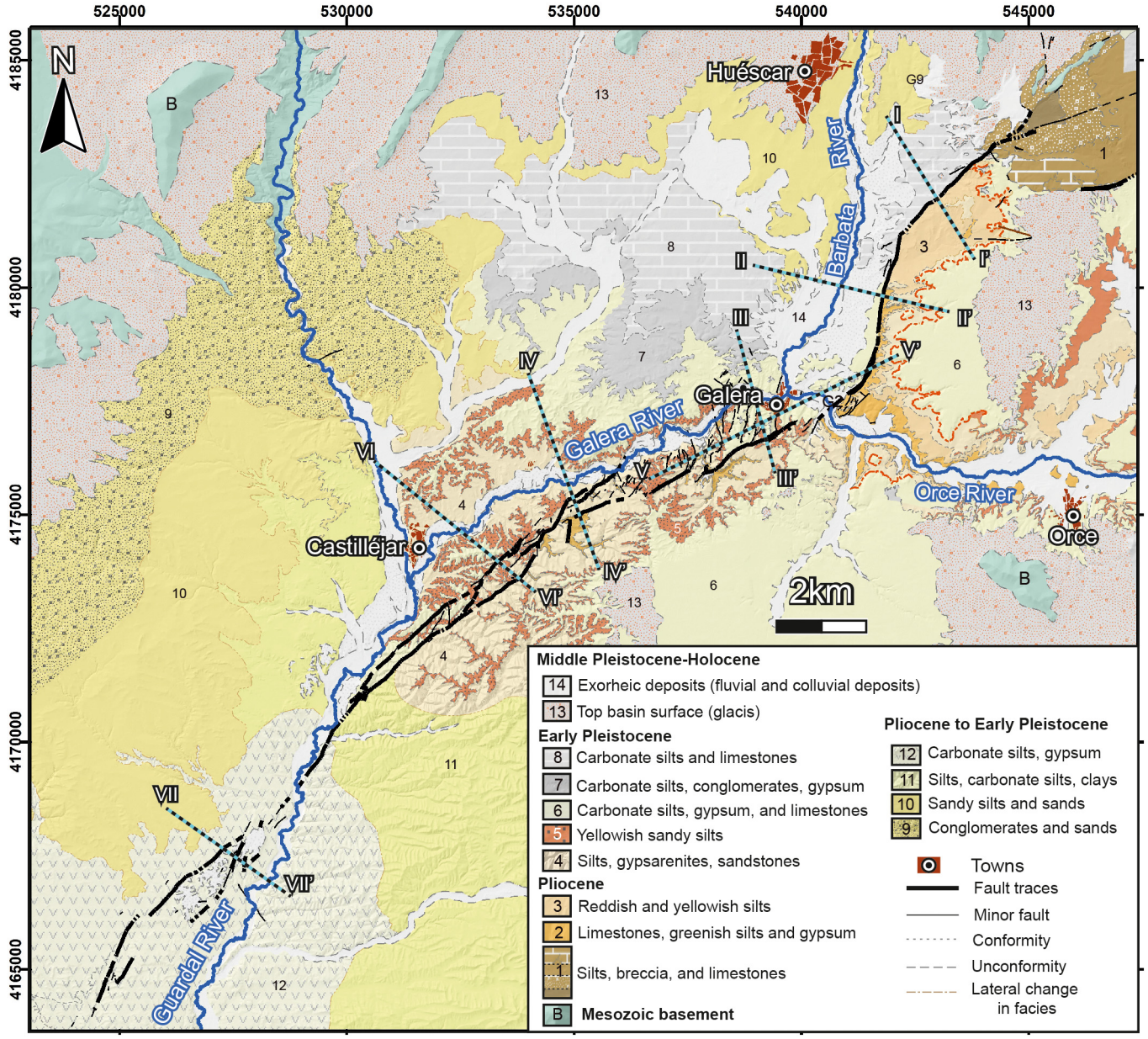

Fig. 3. Geological map displaying the GF and the lithostratigraphic units we defined in the study area. Units 1 to 8 are the most representative units of the study area. They change laterally to marginal (units 9 and 10) and central lake (units 11 and 12) facies. The dashed blue lines show the location of the geological cross-sections in Fig. 5. Main rivers (dark blue lines) are also represented.

effects on cross-fault valley geometries (channel deflections, beheading and/or valley asymmetries, e.g., Zhang et al., 2003), juxtaposition or migration of ridges across the fault, development of fault-facing facets (e.g., Duvall and Tucker, 2015), and/or along-space variations in the degree of valley incision. To complement this analysis, we obtained the profile relief ratio (PRR) along the GF (sensu Duvall and Tucker, 2015). The PRR metric quantifies the landscape response to strike-slip motion by comparing the topography close to and far from the fault traces. The PRR is calculated by dividing the maximum local relief found along a topographic profile close to the fault (10% of the total distance from the fault to the main drainage divide) by the maximum local relief found along a topographic profile located further from the fault (50% of the total distance from the fault to the main drainage divide) (Duvall and Tucker, 2015). Thus, PRR values can range between 0 and 1. Lower PRR values reflect catchments with steep fault-facing slopes and low ridge mobility across the fault, i.e., a static upstream response due to a fast slip along the fault; in contrast, higher PRR values (approximately 1) reflect catchments with erased fault-facing facets and a high degree of cross-fault ridge mobility, i.e., a dynamic upstream response due to a slow slip along the fault.

3.3. Analysis of the glacis surface

The glacis surface of the Baza sub-basin is a pre-deformational geomorphic surface developed during the Middle Pleistocene (García-Tortosa et al., 2011). This surface is an excellent geomorphic marker, as it records deformation produced by fault uplift since basin capture. This surface is intensely affected by erosion in the study area, and it is preserved only close to the sub-basin margins and in some flat hilltop locations. To solve this issue, we follow the methodology used by García-Tortosa et al. (2008b, 2011). This method consists of reconstructing the hypothetical morphology that the Middle Pleistocene glacis surface would have today in the absence of erosion or deformation. For this purpose, we used a low-degree polynomial function to trace envelopes that join the preserved glacis surfaces between the sub-

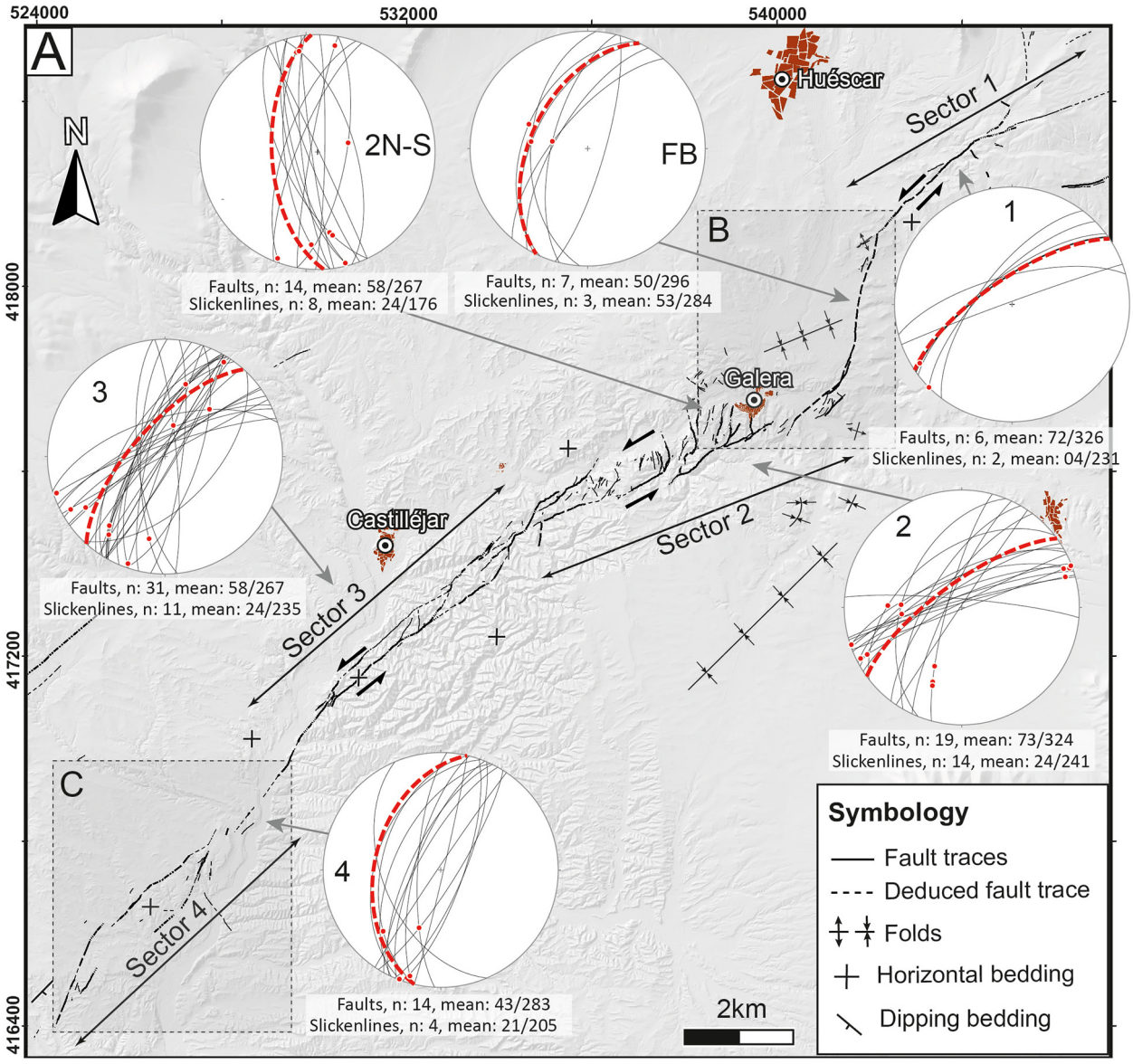
524000
532000
540000
418000
417200
416400
A
N
2N-S
Faults, n: 14, mean: 58/267
Slickenlines, n: 8, mean: 24/176
FB
Faults, n: 7, mean: 50/296
Slickenlines, n: 3, mean: 53/284
Huéscar
Sector 1
B
1
Faults, n: 6, mean: 72/326
Slickenlines, n: 2, mean: 04/231
Galera
3
Faults, n: 31, mean: 58/267
Slickenlines, n: 11, mean: 24/235
Castilléjar
Sector 3
Sector 2
2
Faults, n: 19, mean: 73/324
Slickenlines, n: 14, mean: 24/241
C
4
Sector 4
Faults, n: 14, mean: 43/283
Slickenlines, n: 4, mean: 21/205
2km
Symbology
Fault traces
Deduced fault trace
Folds
Horizontal bedding
Dipping bedding

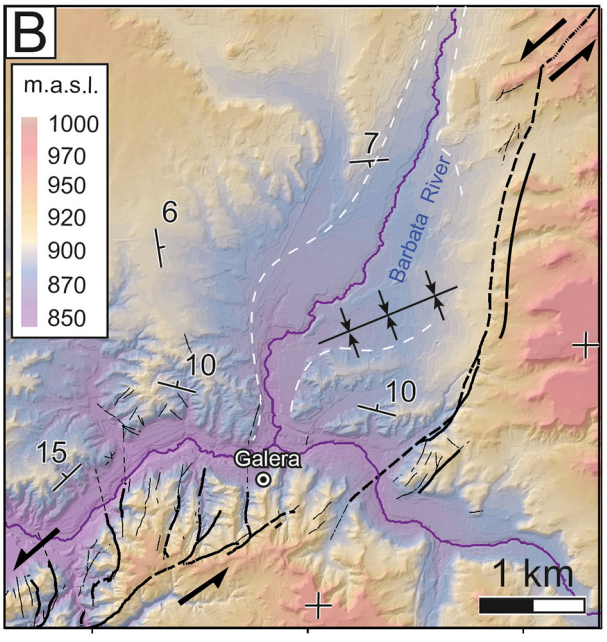
B
m.a.s.l.
1000
970
950
920
900
870
850
7
6
Barbata River
10
10
15
Galera
1 km

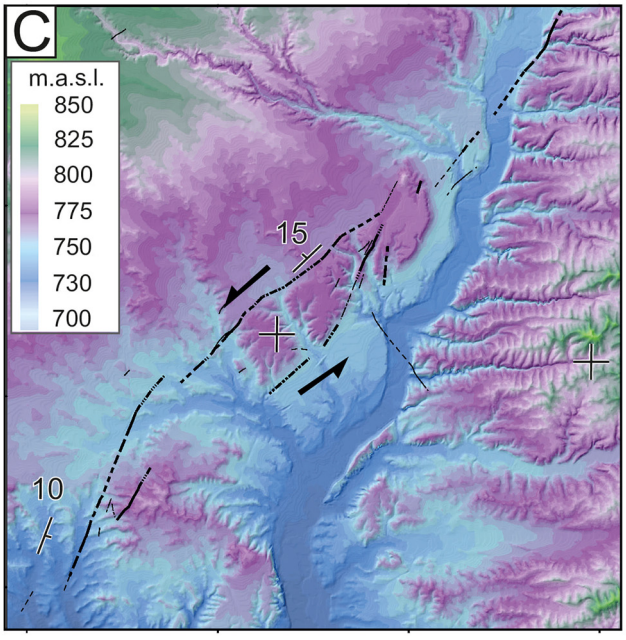
C
m.a.s.l.
850
825
800
775
750
730
700
15
10

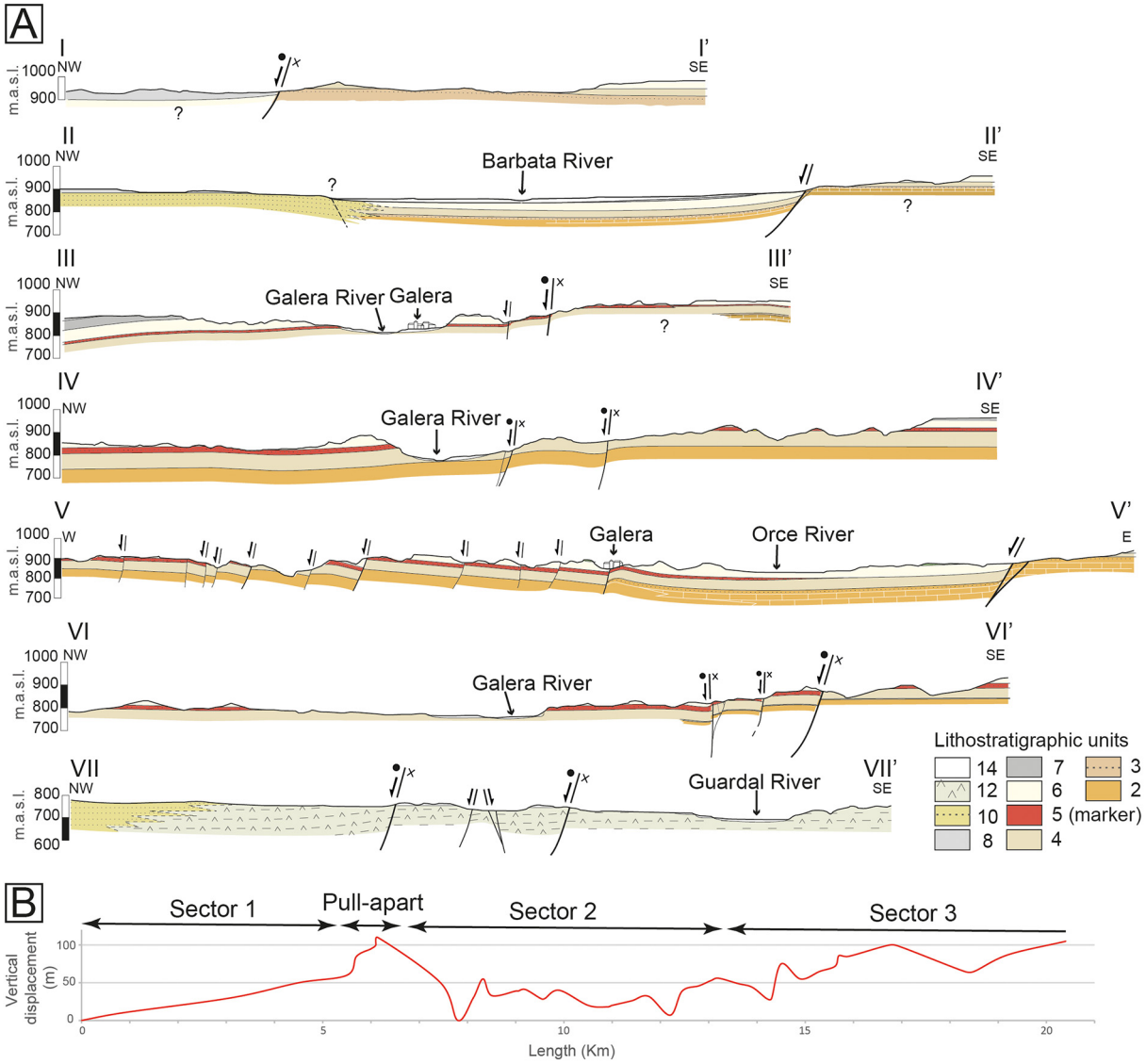

Fig. 5. (A) Geological cross-sections across the GF. Locations and unit description are shown in Fig. 3. (B) Graph showing the measured vertical displacement of the GF using a ca. 2.3 Ma stratigraphic marker (unit 5, in red). Vertical displacement can be measured only along sectors 1 and 2 and part of sector 3.

basin margins. Then, we compare this envelope with the real present-day deformed surface to identify anomalies generated by GF displacement and thus estimate the uplift rate associated with the fault (García-Tortosa et al., 2011). Although this method has already been applied by García-Tortosa et al. (2011) in the Guadix-Baza Basin, they only traced one profile in the Galera region. To estimate the deformation of the glacis surface associated with the GF and fault uplift rate in this study, we reconstruct the glacis surface along 6 basin profiles (including the profile published by García-Tortosa et al., 2011) that cross the GF.

3.4. Drainage network analysis

For the analysis of geomorphic anomalies in the drainage pattern, we extract the drainage network from high-resolution DEMs. From the DEMs, we also delineate catchments in both fault blocks to observe possible effects on their geomorphic parameters related to the relative motion on each side of the fault. For each of these catchments, we calculate the longitudinal profiles of the normalized channel steepness index of their longest streams, asymmetry factor and valley floor width-to-height ratio. The applied indices were originally designed and have typically been used in the assessment of the activity of mountain fronts generated by basin-border faults (e.g., Bull and McFadden, 1977; Keller and Pinter, 2002; Silva et al., 2003; Pérez-Peña et al., 2010a; Matoš et al., 2016). In this work, we test the usefulness of these indices to evaluate the geomorphic effects produced by an active intrabasinal fault.

The morphology of longitudinal river profiles reflects the relationship between erosional processes and tectonic uplift (e.g., Schumm et al., 2000; Keller and Pinter, 2002; Bull, 2009). Concave-up longitudinal profiles reflect stream channels in a steady state, while sublinear, convex, or stepped profiles are related to anomalies derived from tectonic activity, lithologic contrasts, environmental changes, or base-

Fig. 4. (A) Surface geometry map of the GF. Dashed rectangles show the location of the close-ups in B and C. (B) Detail of the pull-apart basin between fault sectors 1 and 2. The white dashed line indicates the widening of the Barbata River valley (C) Detail of the southern termination of the GF in sector 4, where uplifted areas can be observed within the fault zone. (B) and (C) details are displayed over the coloured DEM to illustrate uplifted and depressed areas.

level changes (Hack, 1973; Hovius, 2000; Snyder et al., 2000; Demoulin, 2011; Soria-Jáuregui et al., 2018). Moreover, we calculated the normalized channel steepness index (k_{sn}) (Wobus et al., 2006) in order to detect slope gradient anomalies along longitudinal stream profiles related to fault displacement. The k_{sn} index allows the comparison of stream profiles with highly varying drainage areas. The k_{sn} index is derived from the slope-area regression (e.g., Flint, 1974; Whipple, 2004), defined as:

$$S = KsA^{-\theta}$$

where S is the stream channel slope, K_s is the steepness index (Snyder et al., 2000), A is the drainage area, and θ is the concavity of the longitudinal profile. The k_{sn} index is useful for detecting knickzones, i.e., gradient changes along river profiles that reflect the response of the river system related to base-level falls due to tectonic movements, differential uplift across active structures, and lithologic changes (Wobus et al., 2006; Kirby and Whipple, 2012; Joshi et al., 2021). The geological and structural characterization of the study area allows us to discriminate between knickzones related to erosion steps produced by strong lithologic contrasts or by fault activity.

We also apply the asymmetry factor (AF) (Hare and Gardner, 1985; Keller and Pinter, 2002) to identify possible lateral channel migrations related to fault uplift. The AF determines the degree of asymmetry of catchments, i.e., channel migrations within the catchment area. This index is used to detect tectonic tilting transverse to the flow direction within a drainage basin. This index is defined as follows:

$$AF = | 50 - Ar \cdot 100/At |$$

where *Ar* is the area of the basin to the right (facing downstream) and *At* is the total area of the basin. This equation is expressed as the absolute value minus 50 to avoid possible confusion between catchments draining to the north and catchments draining to the south (sensu Pérez-Peña et al., 2010a). Different AF values permit the classification of catchments as symmetric (AF < 5), gently asymmetric (5 ≤ AF < 10), moderately asymmetric (10 ≤ AF < 15) and strongly asymmetric (AF ≥ 15) (Hare and Gardner, 1985; Keller and Pinter, 2002).

Finally, we apply the valley floor width-to-height ratio (Vf) (Bull and McFadden, 1977). The intention is to detect possible differences in valley incision between fault blocks resulted from tectonic uplift related to the GF. This index was designed to evaluate active tectonics based on the valley geometry in section. It is defined as follows:

$$Vf = \frac{2Vfw}{Eld + Erd - 2Esc}$$

where *Vfw* is the valley floor width, *Eld* and *Erd* are the elevations on both the right and left valley divides, respectively, and *Esc* is the elevation of the valley floor. Low Vf values (Vf < 1) are representative of entrenched V-shaped valleys that are characteristic of areas with active tectonic uplift. In contrast, high Vf values (Vf > 1) reflect U-shaped valleys, which are indicative of areas of low tectonics or tectonic quiescence (e.g., Keller and Pinter, 2002; El Hamdouni et al., 2008). Traditionally, the Vf index is applied to evaluate the uplift of fault-bounded mountain fronts (Silva et al., 2003; García-Tortosa et al., 2008b; Pérez-Peña et al., 2010a). However, in this work, we test the usefulness of the Vf index in an intrabasinal fault that does not generate a mountain front. To detect valley incision anomalies between fault blocks, we calculate Vf values for 5 selected streams in two transverse profiles located 250 m upstream and downstream from the fault zone.

4. Characterization of the Galera Fault

The GF has previously been described as an approximately 30 km-long fault zone striking SW-NE and dipping steeply to the NW or even vertically. We differentiate two main fault blocks: a southern block and a northern block. The minor vertical component of displacement of the GF is responsible for the uplift of the southern block and the subsidence of the northern block.

The GF offsets lower Pliocene to Holocene deposits, affecting both the marginal and central lake facies of the Baza paleolake (Figs. 3, 5 and 6A and B) and exorheic deposits, such as fluvial terraces (Fig. 6C). In this work, we define and map 14 informal lithostratigraphic units (Fig. 3). The ages of the deposits are extracted from previous studies (e.g., Vera et al., 1985, 1994; Soria et al., 1987, 1999; Martín-Suárez, 1988; Alberdi et al., 1989; Agustí and Martín-Suárez, 1984; Garcés et al., 1997; Freudenthal et al., 1998; Oms et al., 2000, 2011; Gibert et al., 2006; Gibert et al., 2007a; Maldonado-Garrido et al., 2017; Piñero and Agustí, 2020). Lithologies in the study area consist mostly of highly erodible lacustrine rocks belonging to the Baza sub-basin sedimentary infill (such as silts, marls, sandstones, and gypsum), which crop out in both fault blocks. Moreover, the most recent infill deposits (units 7 and 8) crop out mainly in the northern fault block (Fig. 3).

From our structural map (Fig. 4), we observe that the surface geometry of the GF is the result of its main strike-slip component (analogous to the geometric patterns developed during Riedel experiments; Riedel, 1929; Tchalenko, 1970). The GF is characterized by structural features that reflect a left lateral sense of displacement (sensu Massironi and Kim, 2015).

We divide the GF into four sectors based on the surface geometry of the fault array (Fig. 4A). Sector 1 strikes SW-NE to WSW-ENE and consists of a single major fault strand with extensional horsetail splays in the NE termination of the fault. Sector 2 is formed by a WSW-ENE-striking fault zone of fault strands arranged in a right-stepping en echelon pattern separated by contractional stepovers. From this fault zone, a set of N-S fault strands branch out and extend N, forming a damage zone of variable width (Figs. 5 and 6E). Deformation along sector 2 has produced an overall tilt towards the N and NW in the northern block of the GF (sections III–III′ and IV–IV′ in Fig. 5) and hectometric- to kilometric-scale gentle folds in the southern block (Fig. 4A). Sector 3 strikes SW-NE, and deformation is distributed along an anastomosing fault zone interpreted as an extensional strike-slip duplex. A gentle N-dipping monocline is observed in the northern block because of the vertical displacement of the GF (sections VI–VI′ in Fig. 5). Sector 4 strikes SW-NE and is arranged in a very segmented en echelon pattern that conforms to the SW fault termination. Deformation in sector 4 is accommodated by hectometric-scale drag, and rollover folds have developed in the northern block (section VII–VII′ in Fig. 5). The most remarkable structural feature of the GF is the kilometric-scale, N-S left fault-releasing bend between sectors 1 and 2 in which a hanging wall and a pull-apart basin are developed (Fig. 4B). The N-S faults and northward tilting observed in sector 2 are the result of subsidence related to this pull-apart basin. We do not consider these fault sectors as different seismogenic fault segments, as they do not comply with the required geometric (Boncio et al., 2004; Field et al., 2015) and kinematic (Chartier et al., 2019) segmentation criteria.

Regarding fault kinematics, previous studies have provided evidence and have quantified the left-lateral component of displacement of the GF from kinematic indicators (slickenlines) (García-Tortosa et al., 2007) and GPS data (Alfaro et al., 2021). In this study, we found slickenlines oriented horizontally to obliquely, which reflects that the fault strands have a main horizontal and minor dip-slip component of displacement (Figs. 4A and 6D). We also found slickenlines indicating pure dip-slip along the left fault bend between sectors 1 and 2 (Fig. 4A).

From offset stratigraphic markers, we estimate the deformation produced by the dip-slip component of the GF (Fig. 5). Stratigraphic markers in the study area are vertically displaced in sector 1, sector 2 and a part of sector 3. The homogeneous sedimentary succession does not allow us to measure fault throw in the SW part of sector 3 and in sector 4. The stratigraphic marker we use for determining the vertical fault offset is the top of unit G5/base of unit G6 (Fig. 3), whose age is ca. 2.3 Ma (Garcés et al., 1997) due to its lateral

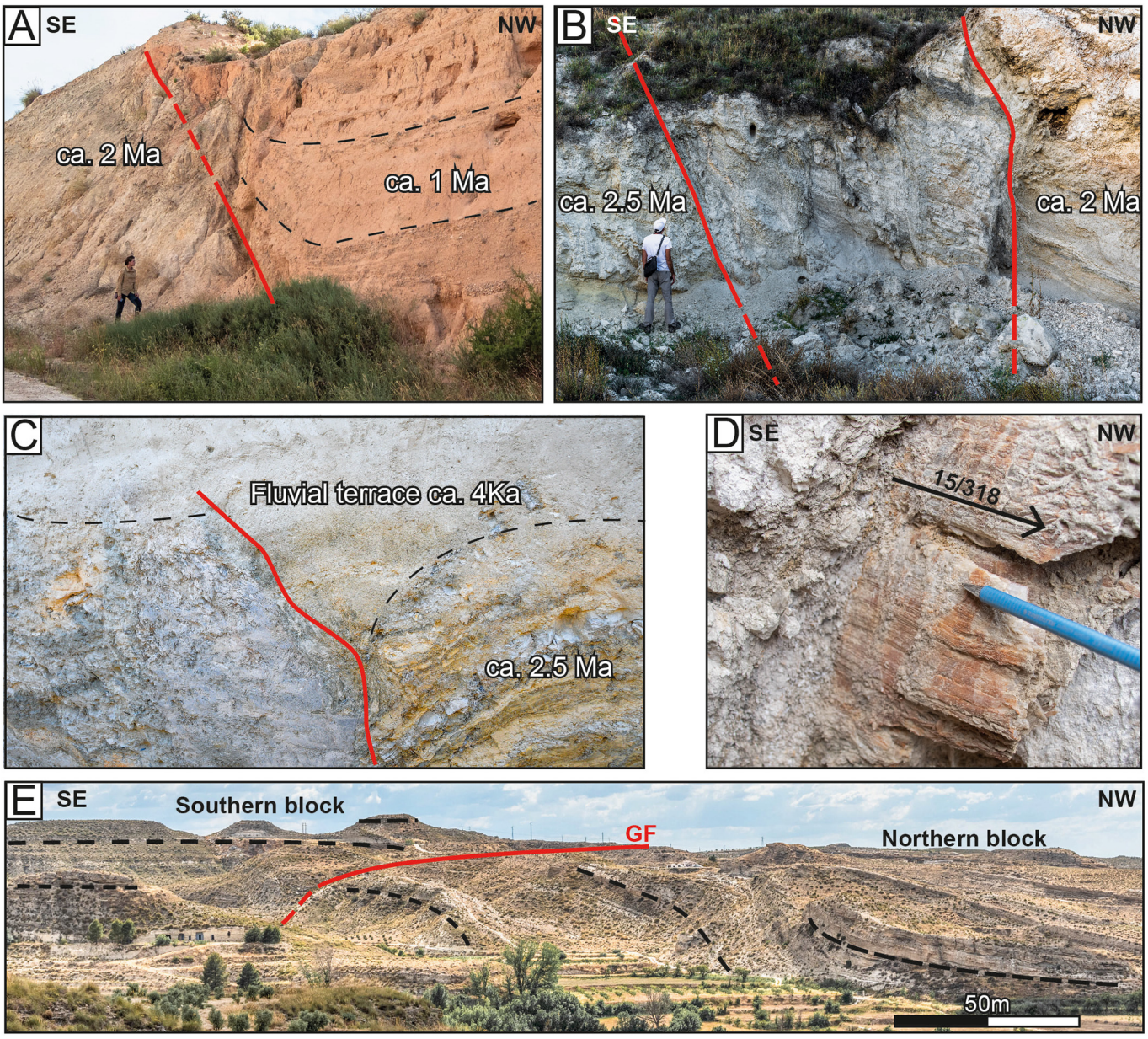

Fig. 6. (A) Fault strand of the GF in sector 1. The fault zone is formed by a single strand. (B) Outcrop of the GF in sector 2. The fault zone consists of a deformation band due to the interaction between several fault strands. (C) A strand of the GF offsetting recent Quaternary fluvial terraces in sector 3. (D) Oblique slickenlines along the SW-NE fault strands of the GF. (E) Northward tilting in the northern fault block related to pull-apart basin subsidence between sectors 1 and 2. Numerical ages of the deposits are extracted from previous studies (e.g., Maldonado-Garrido et al., 2017 and references therein).

continuity in the study area. Vertical displacements range from a few tens of metres to 100 m, with a maximum in sector 3 and along the left fault bend (Fig. 5B).

5. Morphometric analysis

5.1. Topographic analysis

We analyse the topography of the study area from the elevation and slope angle maps (Fig. 7) and from the profile relief ratio (PRR, sensu Duvall and Tucker, 2015).

The elevation map (Fig. 7A) shows that the highest areas (other than the basin margins) correspond to the preserved glacis surface, which also presents the lowest slope angle values (Fig. 7B). In contrast, the lowest areas extend to the SW of the study area, where the fluvial drainage system has incised more deeply into the Baza sub-basin sedimentary infill. However, the most remarkable feature of the elevation map is that it reveals a sharp asymmetry between the southern and northern sides of the main river valleys, i.e., of the Guardal (downstream of the confluence with the Galera River), Galera and Barbata Rivers (Fig. 7A). The relief on the southern side is generally higher than the relief on the northern side. Despite this higher relief in the southern block of the fault, the GF does not present a well-defined mountain front, as it appears highly eroded by the drainage network and has receded more than 2 km in some sectors (Fig. 7A).

From the elevation map, we also identify local topographic features related to the GF traces. The most evident is the southward widening of the Barbata River valley, from a ca. 500 m to 2 km-wide, rhombic-shaped, depressed area in relation with the pull-apart basin between sectors 1 and 2 (Fig. 4B). Other observed features are the high reliefs observed between the GF strands in sector 4 (Fig. 4C).

We also observe differences in the patterns of ridges and fluvial valleys in both the elevation and slope angle maps, especially along sectors 2 and 3 of the GF: on the southern fault block, ridges are

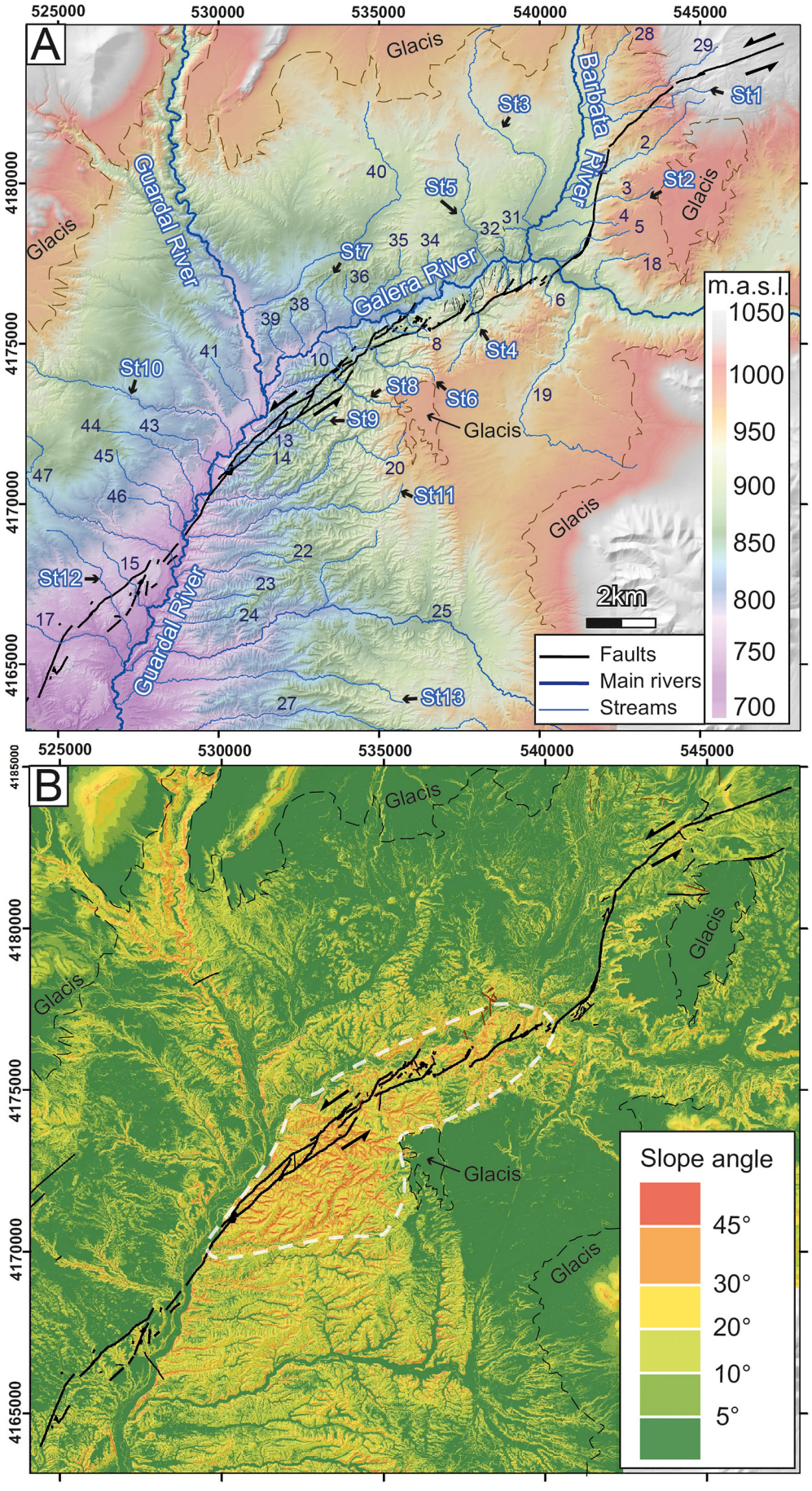
A
B
525000
530000
535000
540000
545000
4185000
4180000
4175000
4170000
4165000
Glacis
Guardal River
Galera River
Barbata River
St1
St2
St3
St4
St5
St6
St7
St8
St9
St10
St11
St12
St13
m.a.s.l.
1050
1000
950
900
850
800
750
700
2km
Faults
Main rivers
Streams
Slope angle
45°
30°
20°
10°
5°

sharp, and valleys are narrower and deeper, showing steep slopes (30–45°); and on the northern fault block, ridges are generally smoother, and valleys are wider and less deep, showing gentler slopes (10–20°) (Fig. 7A and B).

Topographic analysis allows us to identify anomalies in the geometry of cross-fault ridges and fluvial valleys. From the elevation map we observe that the upstream fault block (southern block) does not present fault-facing facets adjacent to the fault traces. Consequently, ridges, i.e., valley divides, are continuous and extend across the fault zone (Fig. 8A). The absence of facets is also evidenced in the strike-parallel topographic profiles we traced along the different sectors of the GF: both the near to and far from fault profiles share very similar high reliefs, yielding high PRR values (close to 1) (Fig. 8B). Regarding cross-fault valley anomalies, we only identify them to the south of the main Galera River valley along the fault zone in sectors 2 and 3. In these sectors, we identify subtle geomorphic features that could be interpreted as steep, left-laterally deflected stream channels and valleys subparallel to the fault strike (Fig. 8A).

5.2. Analysis of the glacis surface

The modelled glacis surface reveals that the vertical dip-slip component of the GF is responsible for the displacement of the glacis surface. The performed analysis allows us to estimate the vertical offset of the glacis and the vertical uplift rate of the GF along sectors 1 to 3. However, the method used (García-Tortosa et al., 2008b, 2011) is not applicable in sector 4 because of the high uncertainty derived from the long distance between the preserved glacis surfaces and the high volume of eroded material in the central part of the subbasin (where the GF is located). Therefore, we estimate the vertical offset of the glacis at 20 ± 5 m in sector 1 (P1 in Fig. 9). Along the fault bend between sectors 1 and 2, the vertical displacement of the glacis surface increases to 75 ± 15 m (P2, Fig. 9). In this fault bend, the vertical displacement of the modelled glacis surface is related to the fault throw, and a gentle rollover fold develops in the northern block. In sector 2, the vertical displacement ranges between 40 ± 5 and 50 ± 5 m (P3 and P4, Fig. 9). These values agree with the displacement estimates of García-Tortosa et al. (2011) in this sector (equivalent to profile P4 in Fig. 9). The displacement observed in sector 2 is mostly related to folding in both fault blocks, as the modelled glacis surface describes a gentle anticline and a pair of synclines (P3 and P4, Fig. 9). In sector 3, we estimate the glacis offset between 85 ± 25 and 90 ± 30 m (P5 and P6, Fig. 9). In this case, the degree of uncertainty is higher as the erosion is more accentuated to the SW. In sector 3, the deformation is related mostly to the fault offset but also to the gentle tilting towards the south. Knowing these approximate vertical glacis surface displacements and considering a minimum age for basin capture ranging between 500 and 600 ka (Gibert et al., 2007b; García-Tortosa et al., 2008a), we estimate the fault uplift rates for each fault sector.

Uplift rates are lowest in sector 1 (ca. 0.03 mm/yr) and highest in sector 3 (0.18 ± 0.04 mm/yr). The obtained values are slightly different from those obtained by García-Tortosa et al. (2007, 2011), which range between 0.08 and 0.24 mm/year in sector 2 (equivalent to our profile P4, Fig. 9). These differences relate to the different ages assigned by these authors to the glacis surface (a minimum of 205 ka and a maximum of 600 ka). Moreover, the vertical displacement amount we obtained using the glacis surface as a marker is slightly different than the vertical displacement we estimated using the stratigraphic markers (Section 4; Fig. 5B). These differences may be related to uncertainties in the glacis surface modelling and/or to age assignment of the used marker (recent markers are less deformed). They could also be related to the fact that when we estimate displacement from stratigraphic markers, we only consider the fault throw (Fig. 5), but when we use the glacis, we include both the fault throw and folding (Fig. 9).

5.3. Drainage network analysis

We perform an analysis of the drainage network pattern and calculate a series of geomorphic indices for the catchments and streams (Table 1), including the k_{sn} and longitudinal profiles (Figs. 11 and 12), AF (Fig. 13), and Vf (Fig. 14) indices.

The study of the drainage network pattern reveals that the main rivers in the study area (Barbata, Galera and Guardal Rivers) run generally subparallel to the GF traces (Fig. 10). However, in sector 4, the Guardal River crosses through the fault zone, decoupling from the GF. We attribute this decoupling to the westward tilting produced by the vertical displacement of the normal Baza Fault (of more than 2000 m, Alfaro et al., 2008; García-Tortosa et al., 2008b, 2011; Haberland et al., 2017; Medina-Cascales et al., 2020), located to the west (Fig. 1).

Moreover, the drainage network map shows differences between the catchments located on the northern and southern fault blocks (Fig. 10). Cross-fault catchments from the southern fault block present, in general, shorter main streams. In addition, the main streams of these catchments initiate from the glacis and flow in all directions, displaying a radial pattern in sectors 2 and 3 (Fig. 10). Another feature is the observed widening, in sectors 2 and 3, of some cross-fault catchments upstream from the fault zone (Fig. 8A). In contrast, catchments located in the northern fault block present, in general, longer main streams. Moreover, they initiate in the northern subbasin margin.

Longitudinal and k_{sn} index profiles were extracted for the main channels of 13 catchments along the four sectors of the GF (St1 to St13, Figs. 7A and 11). All of them correspond to tributary streams draining into the main rivers. In general, most streams have nearly sublinear to slightly concave-up profiles (Fig. 11A). Some streams present convexities along their profiles (e.g., St3 to St6, Fig. 11A). The most noticeable feature is that, in general, cross-fault streams have steeper profiles (Fig. 12). Marked knickzones, which coincide with local k_{sn} maxima, are observed in almost all longitudinal profiles (Fig. 11). Considering the geometry of the fault traces (Fig. 4A) and the geology of the study area (Fig. 3), these slope gradient anomalies and k_{sn} maxima are mainly related to erosional steps. These steps are generated in many cases by strong lithologic contrasts, e.g., between a siltstone and a limestone bed. Other strong gradient anomalies have an anthropogenic origin, e.g., a road crossing a stream (e.g., St3 and St10). Only two profiles (St4 and St12) show steps and k_{sn} maxima that are coincident with fault traces (Fig. 11A).

The AF was calculated for all catchments within the GF and its vicinity (Fig. 13A). Values obtained for cross-fault catchments in sector 1 and the fault bend show an overall asymmetry to the NW (1 to 5 and 18 in Fig. 13A and Table 1). Moreover, the AF of cross-fault catchments in the western parts of sectors 2 and 3 indicate, in general, asymmetries to the N and NNW (7 to 14 in Fig. 13A and Table 1). Some catchments located to the east that drain into the Orce River show asymmetry to the east (6 and 19 in Fig. 13A and Table 1), while a southward asymmetry is observed in the El Margen River catchment (25 in Fig. 13). Conversely, catchments to the north of the Galera River that are situated in the northern block of the GF are generally asymmetric to the SE (30 to 34 and 41 in Fig. 13A and Table 1). Finally, values from catchments in the western part of the study area reflect asymmetries to the SW (15, 17, and 42 to 47 in Fig. 13A and Table 1). The main Barbata River also has a marked asymmetry downstream, defined by a right deflection

Fig. 7. (A) Elevation and (B) slope angle maps extracted from high-resolution DEMs. In the elevation map, the main rivers and longest secondary streams are numbered. St1 to St13 are the streams used in the morphometric analysis. The white dashed line in the slope map indicates the area with the highest slope angle values in sectors 2 and 3. The black dashed line represents the base of the top basin surface (glacis).

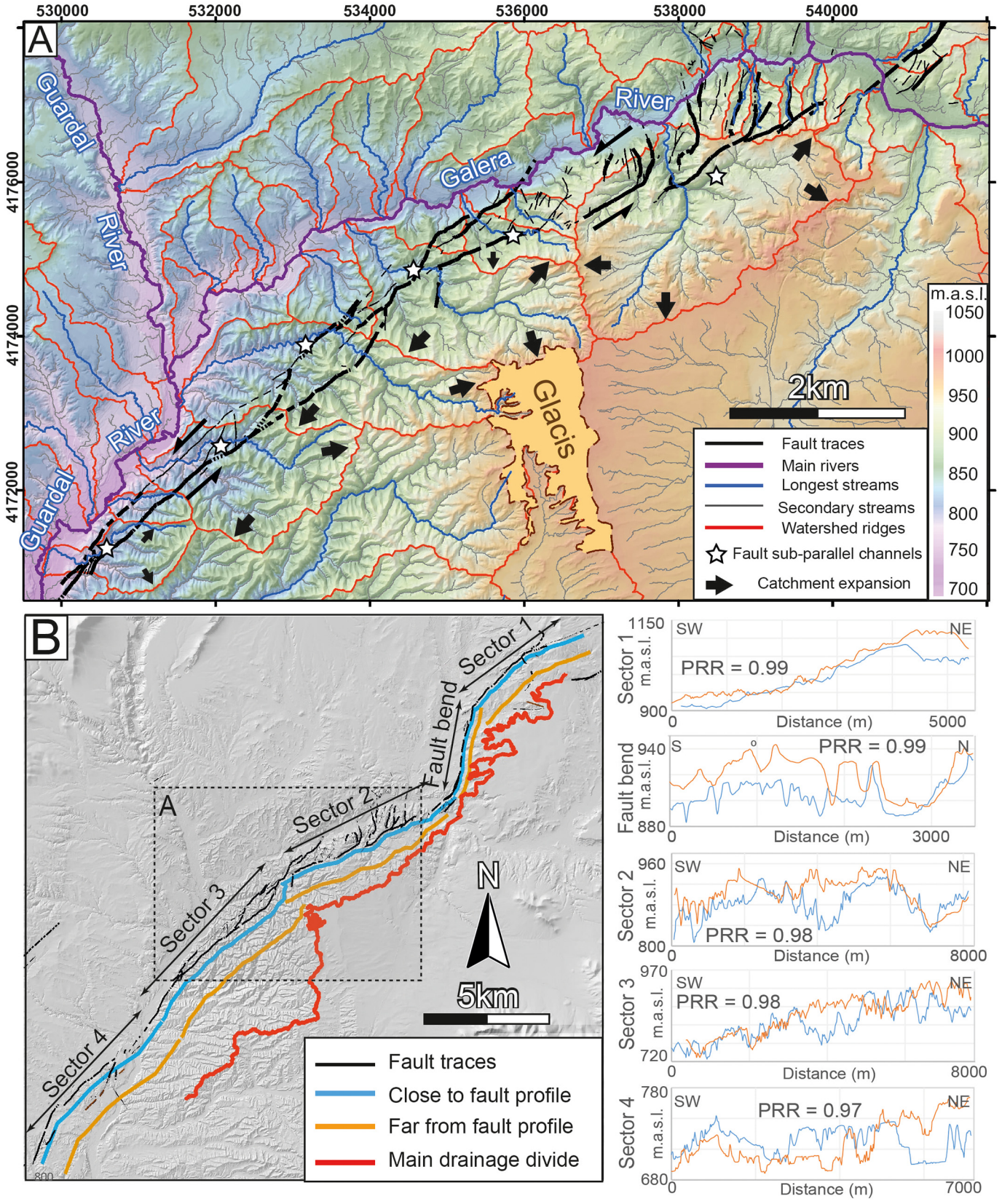

Fig. 8. (A) Close-up of catchments along sectors 2 and 3. The effects of the landscape response to the horizontal displacement of the GF: channel deflections, fault-strike-subparallel channels, ridges extending across the fault, and catchment widening upstream from the fault. Glacis is the term we use for the top basin surface. (B) Strike-parallel topographic profiles near (blue line) and farther (orange line) from the fault, from which the PRR is calculated for the four fault sectors.

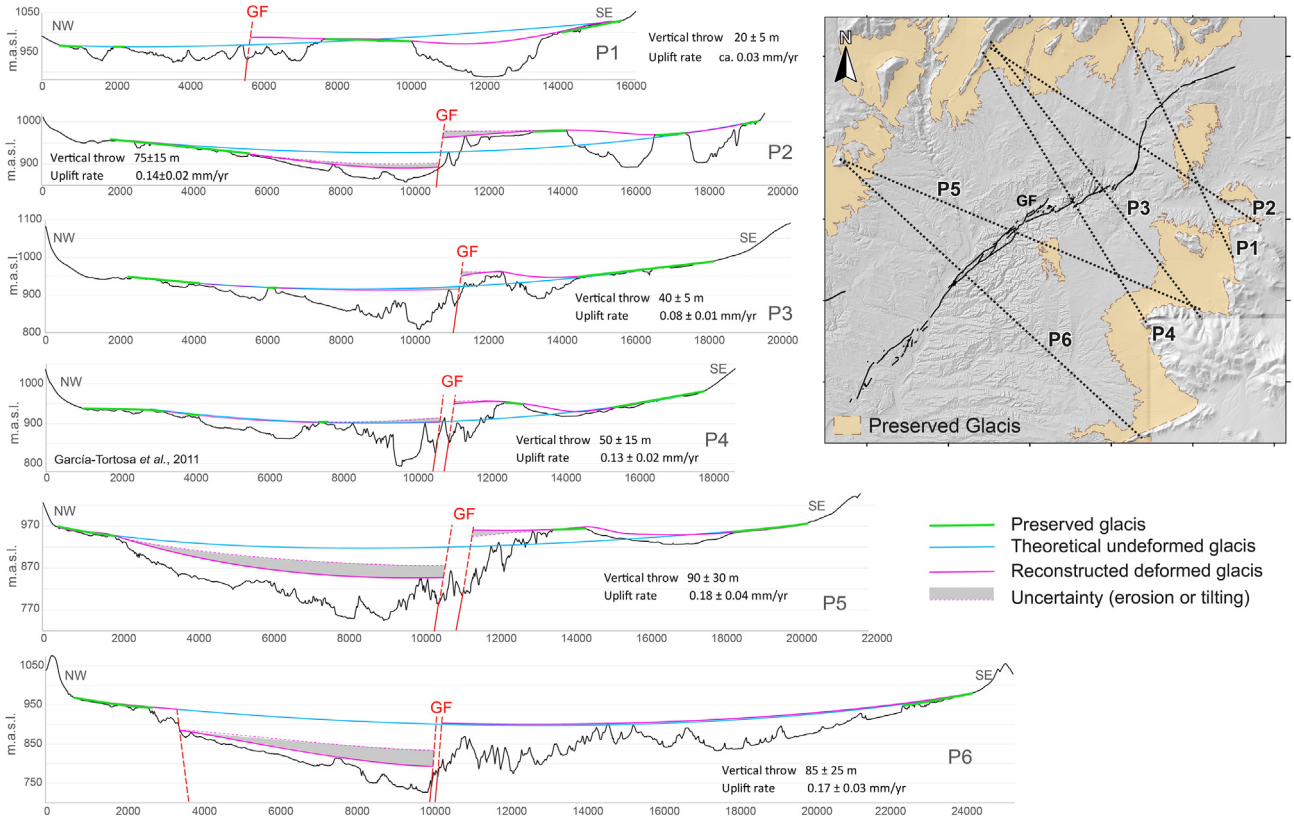

Fig. 9. Glacis surface analysis. Topographic profiles showing the theoretical uneroded and undeformed glacis (top basin surface) (blue line) and the reconstructed deformed glacis (pink line). The dotted pink line with the grey shaded area represents the uncertainty derived from possible glacis erosion. The position of the profiles is indicated in the inset map.

close to its confluence with the Orce River (Fig. 13B), as a response to tectonic tilting in the pull-apart basin (Figs. 4B and 6E) (e.g., Keller and Pinter, 2002).

The calculation of the Vf index in 5 stream channels (St1, St2, St6, St8, and St12, Fig. 14A) reveals that, in general, Vf values are lower when streams flow through the southern block, i.e., they present more V-shaped geometries in cross section (St1, St2, St6, and St8 in Fig. 14A). When these streams cross the fault zone and reach the northern block, Vf values increase, i.e., their valleys present more U-shaped geometries in cross section. In sector 4, stream St13 has high Vf valleys in both the northern and southern blocks but lower Vf values within the fault zone (Fig. 14A). In addition, Vf values obtained for the southern block are lower in sector 3 and higher in sectors 1 and 4, reflecting a lower entrenchment of valleys towards the fault terminations (St1 and St12, Fig. 14A).

6. Discussion

6.1. Tectonic geomorphology of the Galera Fault

The geomorphic characterization of active intrabasinal faults has not been previously addressed through the application of morphometric analyses. In marine or endorheic basins, this may be because the surface expression of this type of fault is obscured by active sedimentation. In the case of captured basins, the nature of recent infill sediments in both fault blocks (usually highly erodible rocks) makes fault characterization challenging due to the poor preservation of tectonic effects on the landscape, especially in regions where the fault is obscured by a highly erosive climate. This is even more difficult in the case of slow-moving faults (<1 mm/yr), such as the GF. Although the GF reunites most of these adverse conditions, the Middle Pleistocene capture of the Guadix-Baza Basin allowed the exposure of the fault structure and the development of its surface expression. The results of our morphometric analysis provide evidence of how this active slow-moving, intrabasinal fault influences the development of recent Quaternary landscapes.

6.1.1. Landscape response to slow-moving intrabasinal faulting

In the case of the GF, slow slip rates in combination with the high erodibility of the sedimentary deposits in both fault blocks have favoured a rapid landscape response to fault activity. This idea is supported by a series of geomorphic evidence that are indicative of a rapid pace of landscape adjustment to a state of disequilibrium induced by the slow horizontal and vertical slip components of the GF.

High PRR values (approximately 1) indicate similar near-to-fault and far-from-fault topography (Fig. 8B). This suggests that topographic effects produced by fault motion, such as sharp fault-facing facets or offset cross-fault ridges, are rapidly erased because of a dynamic landscape response to slow horizontal fault displacement (stages 1 and 2 in Fig. 15) (sensu Duvall and Tucker, 2015).

Other evidence of the rapid landscape response to the fault slip is that, despite uplift related to the vertical component of the fault, the GF does not present a clearly observable mountain front. According to Bull and McFadden (1977), when the present erosional front is more than 1 km away from the fault, the mountain front is considered tectonically inactive. However, this statement is applied to basin-border faults with well-developed mountain fronts, where the uplifted block is usually formed by hard basement rocks. The case of the GF is different, as it juxtaposes highly erodible deposits from the basin infill (Figs. 3 and 5). In addition, the uplift rate is very low. Therefore, as the fault displacement uplifts the relief, it is rapidly erased by the development of the intricate drainage system in the study area, resulting in a receded

Table 1
Parameters of the streams and catchments analysed in this study: stream position with respect to the GF, fault sector, length of the longest stream, headwater elevation, drainage area of the catchment, and asymmetry factor (AF) of each catchment. Selected streams for the application of k_{sn} and Vf indices are remarked in blue. Streams are ordered according to their position with respect to the fault (cross-fault, southern block or northern block).

Stream	Position	Sector	Length (km)	Headwater elevation (m.a.s.l)	Drainage area (km²)	AF
1 (St1)	**Cross-fault (SE-NW)**	**Fault bend**	**6.67**	**979**	**2.74**	**3.28**
2	Cross-fault (SE-NW)	Fault bend	6.68	1042	5.77	17.59 (NW)
3 (St2)	**Cross-fault (SE-NW)**	**Fault bend**	**3.75**	**969**	**1.48**	**4.73**
4	Cross-fault (SE-NW)	Fault bend	3.47	965	1.61	5.90
5	Cross-fault (SE-NW)	Fault bend	3.00	963	1.1	15.45 (NW)
6	Cross-fault (SE-NW)	2	1.68	938	0.53	10.38 (E)
7 (St4)	**Cross-fault (SE-NW)**	**2**	**3.55**	**952**	**6.28**	**16.08 (NW)**
8	Cross-fault (SE-NW)	2	2.25	930	0.76	22.37 (NNE)
9 (St6)	**Cross-fault (SE-NW)**	**3**	**4.78**	**964**	**3.99**	**8.15 (NNW)**
10	Cross-fault (SE-NW)	3	1.48	880	0.87	5.17
11 (St8)	**Cross-fault (SE-NW)**	**3**	**6.72**	**952**	**4.34**	**18.89 (N)**
12 (St9)	**Cross-fault (SE-NW)**	**3**	**4.08**	**916**	**3.11**	**25.24 (NNW)**
13	Cross-fault (SE-NW)	3	1.20	840	0.38	31.58 (N)
14	Cross-fault (SE-NW)	3	2.83	855	1.13	32.3 (N)
15	Cross-fault (NW-SE)	4	2.83	763	1.89	23.02 (SW)
16 (St12)	**Cross-fault (NW-SE)**	**4**	**5.87**	**800**	**3.15**	**3.97**
17	Cross-fault (NW-SE)	4	6.74	780	12.23	12.14 (SW)
18	Southern block	Fault bend	2.90	958	1.04	9.62 (NW)
19	Southern block (far SE)	2	11.37	976	28.16	16.69 (E)
20	Southern block	3	9.27	956	7.83	13.47 (S)
21 (St11)	**Southern block**	**4**	**8.47**	**927**	**9.82**	**4.99**
22	Southern block	4	5.04	860	3.39	25.81 (N)
23	Southern block	4	3.17	850	1.25	6.8
24	Southern block	4	3.41	830	1.17	1.28
25	Southern block (far SE)	4	22.22	986	51.6	10 (S)
26 (St13)	**Southern block (far SE)**	**4**	**12.21**	**910**	**8.17**	**0.06**
27	Southern block (far SE)	4	20.90	980	20.53	22.4 (N)
28	Northern block	1	3.26	973	6.03	26.29 (NW)
29	Northern block	1	5.02	1105	2.6	8.08 (NW)
30 (St3)	**Northern block**	**Fault bend**	**10.52**	**944**	**13.41**	**8.54 (S)**
31	Northern block	Fault bend	0.97	871	0.29	8.62 (S)
32	Northern block	2	0.98	880	0.3	13.33 (E)
33 (St5)	**Northern block**	**2**	**5.26**	**920**	**8.25**	**13.64 (SE)**
34	Northern block	2	1.90	878	1.1	5.45
35	Northern block	2	3.35	881	2.25	1.11
36	Northern block	3	2.40	836	1.17	10.68 (SW)
37 (St7)	**Northern block**	**3**	**2.44**	**840**	**1.37**	**13.5 (NE)**
38	Northern block	3	1.97	812	0.63	3.97
39	Northern block	3	1.78	814	0.75	16.67 (SW)
40	Northern block	3	11.87	945	35.53	22.31 (SE)
41	Northern block	3	3.00	805	1.17	9.83 (SW)
42 (St10)	**Northern block**	**3**	**10.28**	**940**	**27.6**	**26.56 (SW)**
43	Northern block	3	2.57	790	1.13	6.64 (NE)
44	Northern block	4	4.85	815	3.69	22.63 (NE)
45	Northern block	4	3.87	800	1.7	8.82 (NE)
46	Northern block	4	2.50	767	1.11	24.77 (NE)
47	Northern block	4	11.87	939	16.9	15.38 (SW)

mountain front (Fig. 16A and B). This demonstrates that highly eroded fronts can also be related to active faults.

The application of the k_{sn} index may also indicate a rapid erasing of topographic effects generated by GF uplift (Fig. 16C). Some erosional strong slope gradients (k_{sn} knickzones) located upstream from the fault zone in longitudinal profiles (e.g., in St1, St2, St4, St6, and St8 profiles, Fig. 11) could be interpreted as a result of upwards knickzone migration (e.g., Whipple and Tucker, 1999; Bishop, 2007; Castillo et al., 2014). These migrations are usually produced by headward erosion after sudden base-level falls (Fig. 16C). As the studied streams were generated after Guadix-Baza sub-basin capture, we attribute these base-level falls to fault uplift. Hence, after each episode of tectonic uplift, topographic steps may develop in the streambeds related to fault traces (stage 2 in Fig. 16C). However, the high erodibility of the deposits and the slow uplift rate of the GF would favour the prompt erasing of these steps by headward erosion (stage 3 in Fig. 16C).

From all of this evidence, we observe that rapid landscape adjustments to GF activity result in a masking of many geomorphic effects related to oblique fault displacement. Nevertheless, even in this adverse framework, this study demonstrates how morphometric analyses are an very useful tool to detect geomorphic effects related to slow-moving, intrabasinal fault displacement.

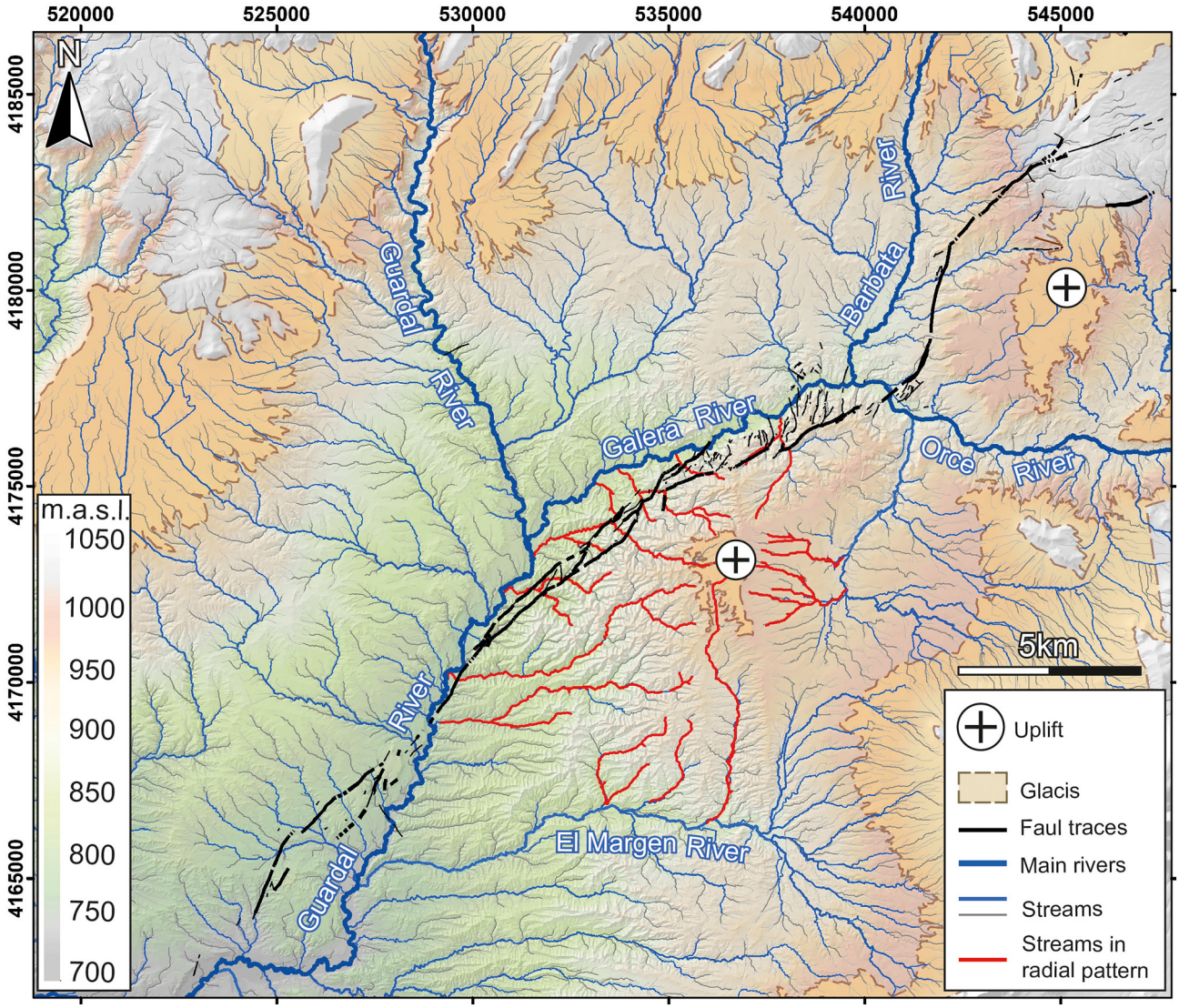

Fig. 10. Drainage network pattern in the study area. The radial pattern of the drainage network observed to the south of the Galera River (red streams) reflects the higher uplift in this area. Glacis is the term we use for the top basin surface.

6.1.2. Geomorphic evidence of horizontal fault displacement

Although the GF presents a main left-lateral slip component (0.5 ± 0.3 mm/yr, Alfaro et al., 2021), the rapid erasing of geomorphic effects is more effective on features generated by strike-slip displacement. The GF shows subtle evidence of the most common features defining the tectonic geomorphology of strike-slip faults, such as the offset of geomorphic markers (streams, alluvial fans, fluvial terraces, and ridges), stream deflections, and fault-parallel channels (e.g., Wallace, 1968; Sylvester, 1988; Keller and Pinter, 1996; Walker et al., 2006; Gürbüz et al., 2015; Zielke et al., 2015; Salisbury et al., 2018). We observe only a few examples of local left-lateral deflections and fault-subparallel channels (Fig. 8A). Apart from these features, we also interpret the downstream widening of the Barbata River valley, related to the pull-apart basin (Fig. 4B), as a result of the transtension generated by the combination of the left-lateral motion of the GF and its geometry (a left fault bend) (sensu Mann et al., 1983) (Fig. 4B).

Another feature reflecting the horizontal displacement of the GF is the widening of catchments upstream from the fault in sectors 2 and 3 (Fig. 8A). This widening is the result of the growth of new channels that initiated from fault-subparallel channel segments. As these fault-subparallel segments grew laterally due to left-lateral displacement of the GF, they acted as local base levels from which new channels developed via headward erosion (stage 2 in Fig. 15). These new channels expanded laterally towards the main drainage divide, increasing the catchment area upstream from the fault, and shrinking the neighbouring catchments (stage 3 in Fig. 15). These widening processes are also a consequence of the rapid landscape adjustment to fault activity, reflecting a vigorous catchment reorganization in response to horizontal fault motion (sensu Duvall and Tucker, 2015).

Moreover, these widened catchments are asymmetric to the N and NW according to the obtained values of the AF index (Fig. 13A). Catchment asymmetries are usually interpreted as a result of lateral channel migrations triggered by tectonic tilting (e.g., Hare and Gardner, 1985; Dhanya and Tiruvanatpuram, 2014; Valkanou et al., 2020), but in this case, we postulate that asymmetries are related to the catchment widening process (Fig. 15). Therefore, although the AF was designed to detect effects produced by vertical fault displacement, in these catchments it may reflect the imprint of strike-slip displacement.

6.1.3. Geomorphic evidence of vertical fault displacement

The secondary vertical component of displacement of the GF (maximum of ca. 0.2 mm/yr, García-Tortosa et al., 2011 and this study) is, however, responsible for generating the most significant landscape effects. In addition to the vertical deformation of the

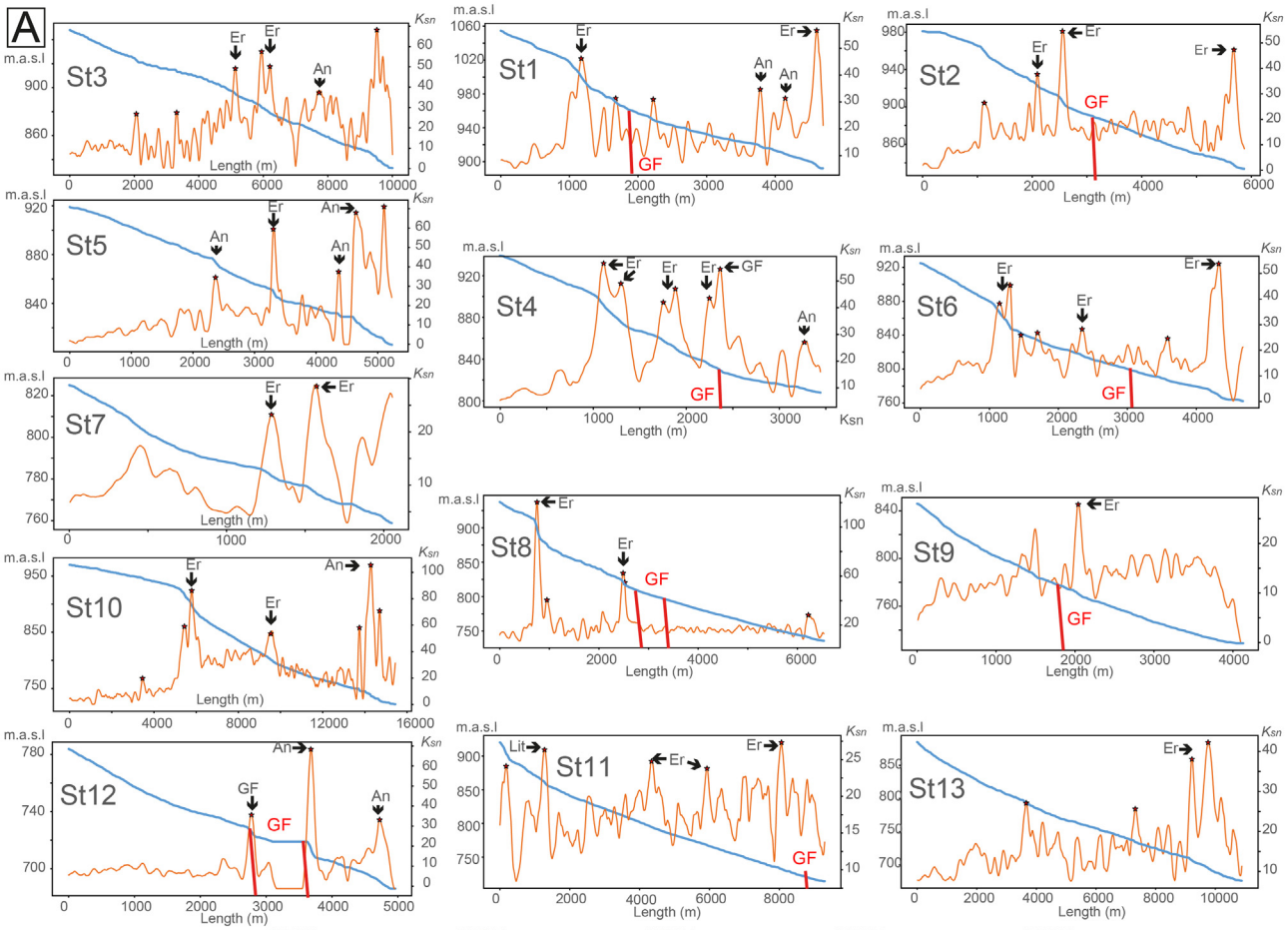
A
St3
St1
St2
St5
St4
St6
St7
St8
St9
St10
St11
St12
St13
m.a.s.l
Ksn
Length (m)
Er
An
GF
Lit

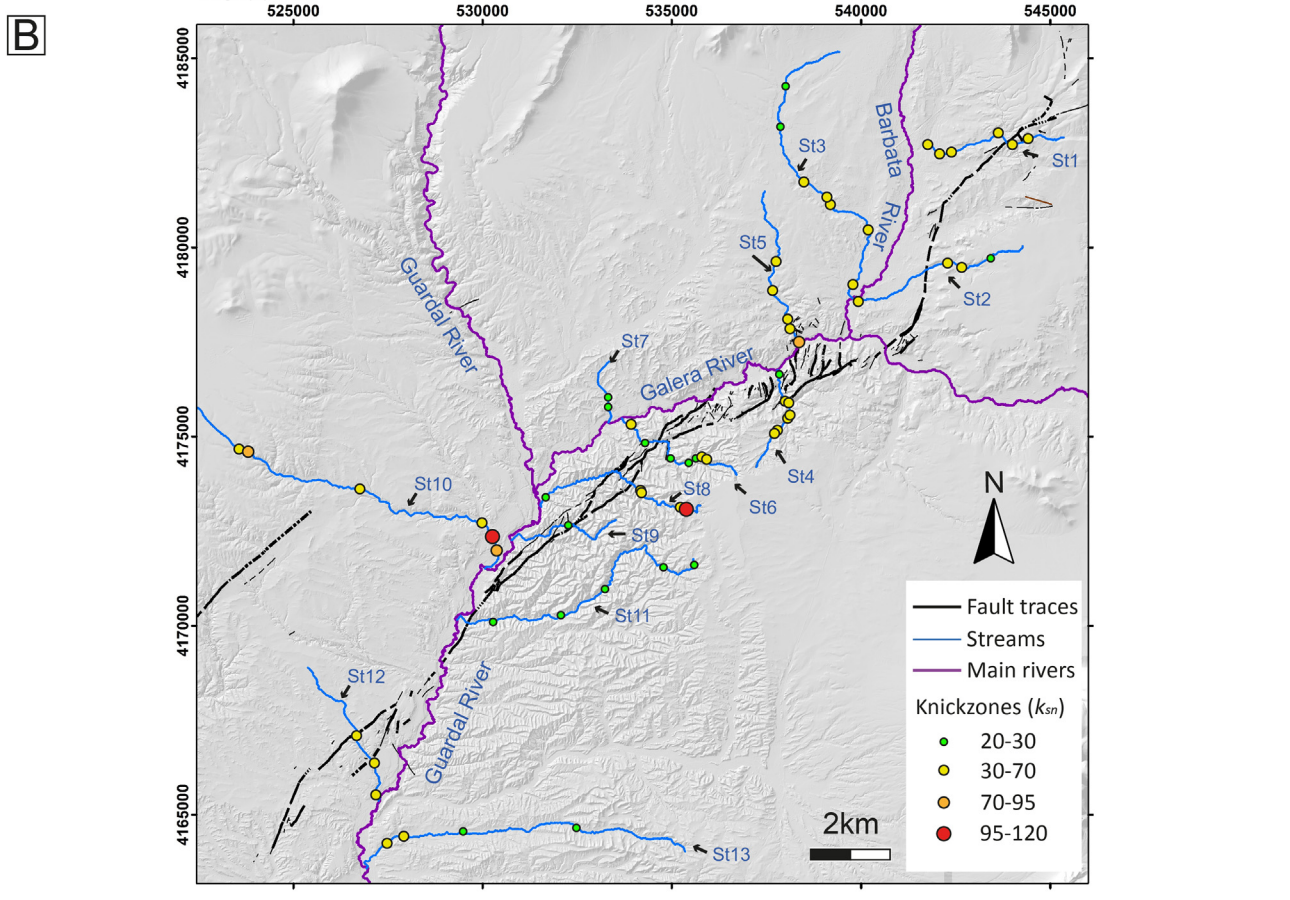
B
525000
530000
535000
540000
545000
4185000
4180000
4175000
4170000
4165000
Barbata River
Guardal River
Galera River
Guardal River
St1
St2
St3
St4
St5
St6
St7
St8
St9
St10
St11
St12
St13
N
2km
Fault traces
Streams
Main rivers
Knickzones (ksn)
20-30
30-70
70-95
95-120

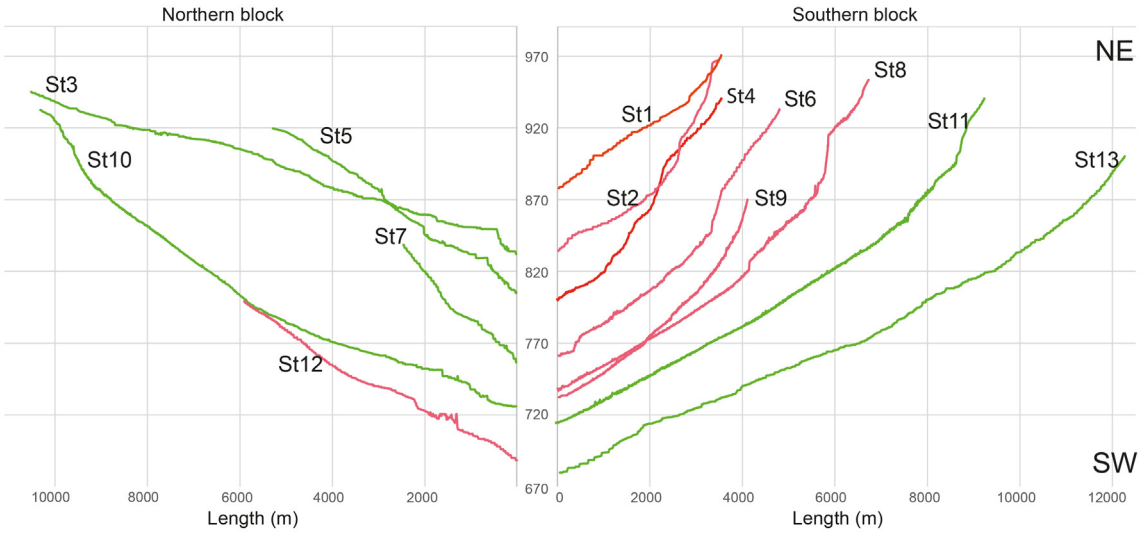

Fig. 12. Comparison of the longitudinal stream profiles between the northern and southern fault blocks. Cross-fault streams (red profiles) are shorter and steeper, reflecting fault uplift.

glacis surface, which is more intense in the central part of the fault (Fig. 9), the uplift of the southern fault block has generated local high relief (Fig. 7A) that represents an intrabasinal topographic anomaly. The elevation of this relief has determined the geometry of the main rivers in the NE sector of the Baza sub-basin (Fig. 10), which flow subparallel to the GF trace along most of its length (Fig. 10).

This topographic anomaly triggered a landscape response that resulted in the observed drainage pattern differences between fault blocks (Fig. 10). On the southern fault block, streams do not initiate from the basin margins but from this tectonically uplifted relief (Figs. 10 and 16A and B). Consequently, due to the short distance between the elevated areas and main rivers (ca. 1 km to 5 km), cross-fault catchments (e.g., 1 to 14 and 20 in Figs. 7A and 13A and Table 1) present, in general, shorter main channels (Figs. 10B, 11, 12, and 16B) and smaller areas (Fig. 13A). The steeper longitudinal profiles of cross-fault streams (e.g., St2, St4, St6, and St9 in Fig. 12) also reflect the effects of fault uplift, while streams flowing far from the influence of the GF in the southern block show gentler and longer profiles (e.g., St13).

Moreover, the Vf index results show that in these cross-fault streams, valley incision is higher in the southern block (Fig. 14) (sensu Keller and Pinter, 2002). These values reflect that despite the low slip rate, fault activity strongly controls valley incision in the study area. The active incision has resulted in narrow, deep valleys with sharp ridges (Fig. 7) that display the characteristic badland landscape of this sector in the Baza sub-basin (Fig. 2D and E), which is only developed on the southern block of the GF (Figs. 7A, 14B, and 16A and B).

In addition, the morphometric analysis reveals that tectonic uplift is higher in sectors 2 and 3. This is evidenced by the drainage network geometry, whereby the radial pattern (Fig. 10) suggests that uplift in these sectors contributes to generating a dome-shaped elevated area (e.g., Pain, 1985; Molin et al., 2004). The higher uplift of this area is responsible for generating eastward and southward catchment asymmetries (Fig. 13A) and higher valley incision, as indicated by the low Vf values (Fig. 14), elevation and slope maps (valleys are deeper and present especially pronounced slopes, Fig. 7). Structural data (Fig. 4A) and glacis surface deformation (Fig. 9) show that this dome corresponds to an actively growing anticlinal fold related to the GF.

On the northern fault block, the relative tectonic subsidence, and the absence of intrabasinal uplifted areas are also reflected by the drainage network. In this case, streams are longer (Figs. 10, 11, 12, and 13A and Table 1), as they initiate from the northern sub-basin margin (ca. 10 to 12 km from the main rivers), and their valleys are less entrenched (Figs. 7, 14B and 16B). In the northern fault block, we interpret lateral channel migrations to the south and SE in response to the tectonic tilting produced towards the pull-apart basin (Fig. 13A).

Apart from the fault vertical displacement, other factors, such as fluvial discharge variations or the riverbed lithology, could also be considered responsible for differences in the drainage network between fault blocks. The Baza sub-basin is characterized by a semiarid climate with low but intense annual precipitation. These conditions, together with the high erodibility of the sedimentary rocks that dominate the study area (Fig. 3), cause erosional processes to be the main agent responsible for landscape configuration (Pérez-Peña et al., 2009). However, given the relatively small size of the study area (ca. 470 km^2), we consider climate and lithology to be homogeneous. Therefore, in the case of the GF, we postulate that tectonic uplift is the key factor controlling drainage differences between fault blocks (Figs. 15 and 16).

In summary, a morphometric analysis typically applied in basin-border faults (e.g., Bull and McFadden, 1977, Keller and Pinter, 2002; Silva et al., 2003; Mériaux et al., 2005; Pérez-Peña et al., 2010a; Ul-Hadi et al., 2013; Gürbüz et al., 2015 Matoš et al., 2016; Yazici et al., 2018, amongst many others) has provided equally valid results in defining the geomorphic expression of a slow-moving intrabasinal fault. The application of the Vf index in a different context has provided valuable results for detecting differences in valley incision between fault blocks, even with the absence of a developed mountain front. The AF has proven helpful not only for evaluating effects related to fault uplift (e.g., lateral channel migrations produced by tilting) but also for detecting geomorphic anomalies related to strike-slip displacement (asymmetries generated by catchment widening, Fig. 15). Moreover, geomorphic indices such as the PRR and k_{sn} have provided useful information regarding the landscape response to the activity of a slow-moving fault offsetting highly erodible deposits.

Despite the usefulness of our analysis, we consider it important to remark on the importance of combining geological, structural, and

Fig. 11. (A) Longitudinal stream profiles (blue lines) and k_{sn} profiles (orange lines) corresponding to the streams used in the geomorphic analysis (St1 to St13). The profiles are not scaled to one another. The scale of these profiles is reflected in their graph axes. Knickzones, which are indicated, are generated by erosional steps (Er), the Galera Fault (GF), or anthropogenic structures, e.g., roads (An). (B) Map showing k_{sn} knickzones related to the analysed streams (St1 to St13). Comparison of the longitudinal stream profiles between the northern and southern fault blocks. Cross-fault streams (red profiles) are shorter and steeper, reflecting fault uplift.

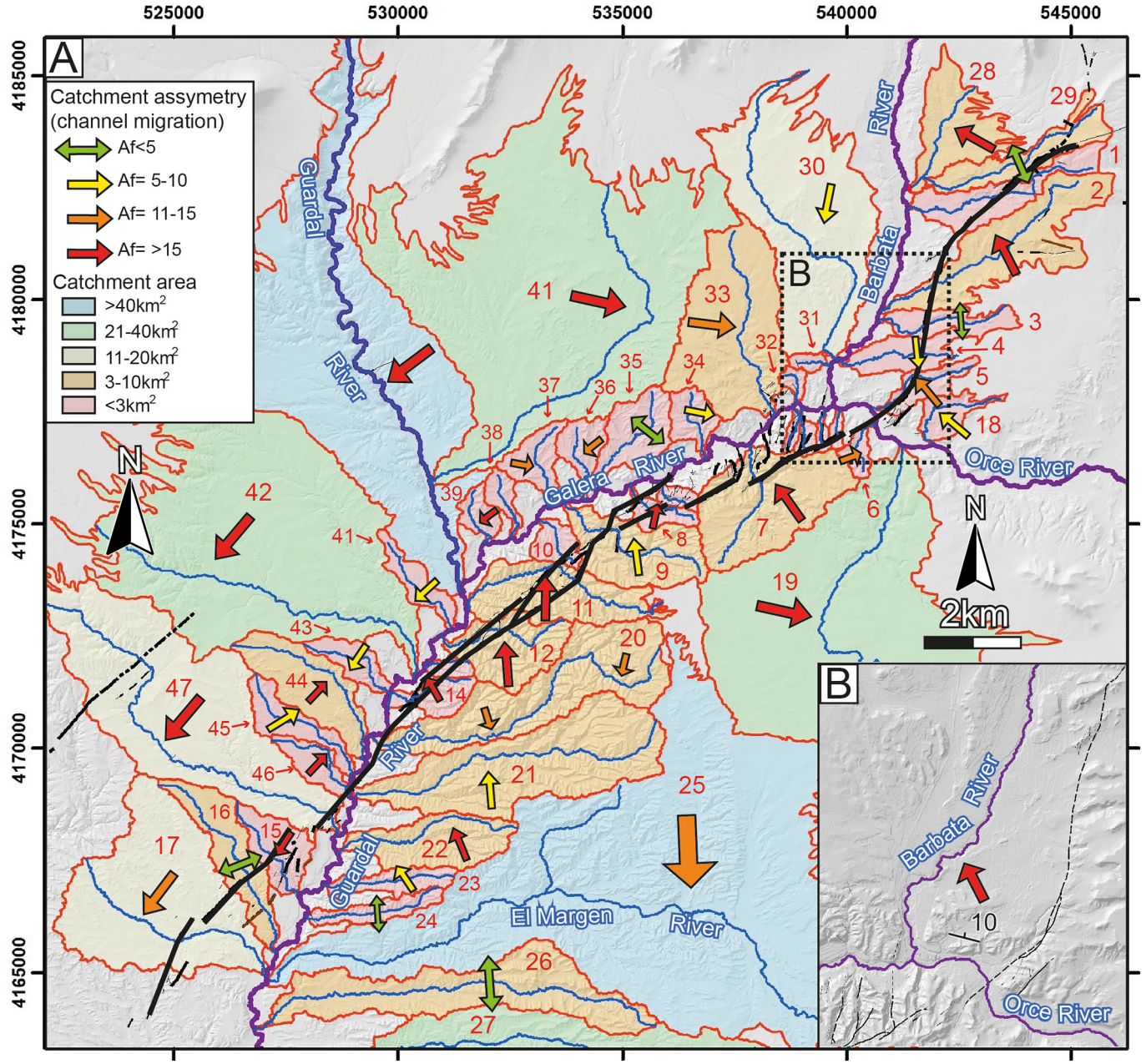

Fig. 13. Digital elevation model (DEM) with the catchments in both fault blocks classified by their area. Smaller catchments dominate the southern block and fault zone, while more extensive catchments are present in the northern block. (B) Close-up of the right deflection of the Barbata River due to tectonic tilting. The arrows show the direction of catchment asymmetry, and their colours reflect the magnitude (classified sensu Pérez-Peña et al., 2010a).

geomorphic analyses. This is particularly important in oblique-slip, slow-moving faults that offset highly erodible rocks. As we described above, although the GF presents a main left-lateral displacement, its geomorphic signature is mainly defined by features related to vertical displacement, as they are better preserved. Therefore, based on its geomorphic imprint and without a previous structural analysis, the GF could be erroneously considered a pure vertical-slip fault. Moreover, knowledge of the detailed geology of the study area is essential to discriminate between geomorphic effects related or not related to fault activity. For example, morphometric analyses based on the application of the k_{sn} index have been previously used in other contexts to detect and delineate fault traces or fault zones in regions with poor exposure conditions (e.g., in Marliyani et al., 2016). In our case study, this index could not be applied for this purpose, as knickzones are mainly related to erosion or anthropogenic structures.

6.2. Relief building in the central Betic Cordillera during the Quaternary: insights from Galera Fault activity

The Betic Cordillera is an evolving collisional orogen with significant relief building (i.e., topographic growth) since the late Miocene. Many studies have focused on the chronology of this mountain building from different approaches. Proposed hypotheses include continuous regional uplift since the late Miocene (Braga et al., 2003; Sanz de Galdeano and Alfaro, 2004), a steady-state topography where uplift is balanced by denudation (Bellin et al., 2014), and episodic uplift (Farines et al., 2015) in which the Lower Pleistocene marks the end of the most recent phase of major relief formation (Stokes et al., 2018). Active oblique-slip faults play an important role in this relief building, related to their vertical displacement and to transtensive and transpressive zones (e.g., Silva et al., 2003; Martínez-Díaz et al., 2012; Pérez-Peña et al., 2010a; Moreno et al., 2015; Martin-Banda et al., 2016). Active oblique-slip faulting occurs in

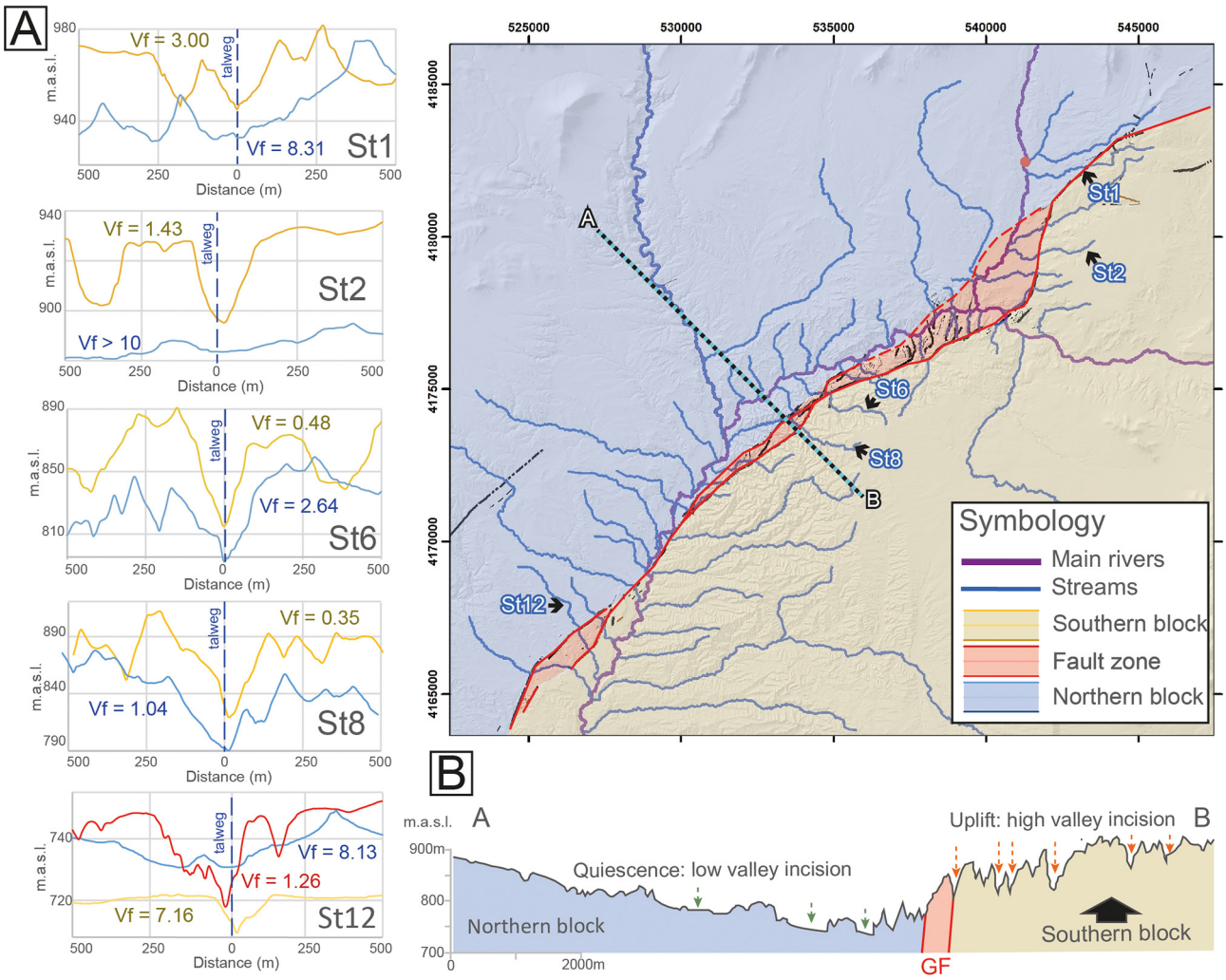

Fig. 14. (A) Charts depicting the transverse topographic profiles and Vf index values extracted from 5 representative streams in the study area. The position of these streams is shown in the map. (B) Schematic topographic profile showing the valley incision differences between the northern and southern fault blocks. The vertical scale is exaggerated. The position of the profile is indicated in the map in (A) by a dashed line.

two main sectors of the Betic Cordillera under different geodynamic conditions: i) the Eastern Betic Shear Zone (EBSZ, Bousquet, 1979; De Larouzière et al., 1988; Silva et al., 1993), and ii) the extensional central Betic Cordillera (Fig. 17).

The EBSZ is the result of tectonic indentation processes in relation to the NNW-SSE convergence of the Nubian and Eurasian plates (Coppier et al., 1989; Palano et al., 2015; Borque et al., 2019). Consequently, these oblique structures present a left-lateral and reverse displacements

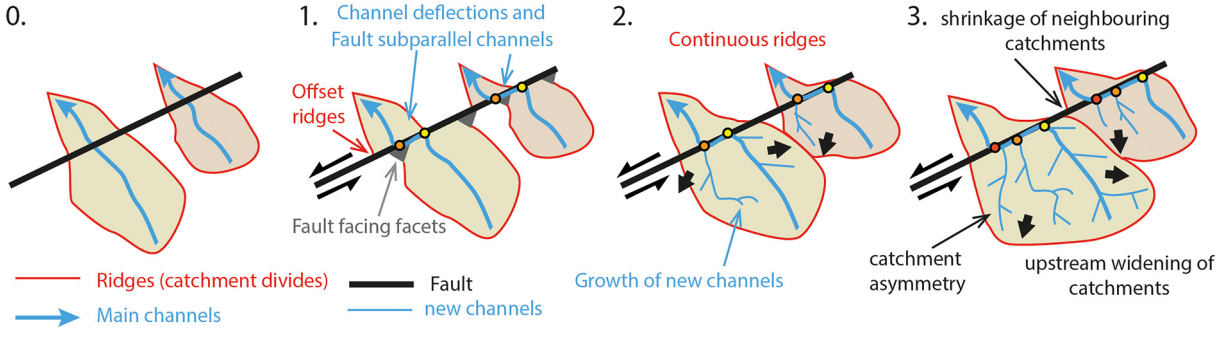

Fig. 15. Schematic sketches illustrating the landscape effects derived from the rapid landscape response to fault displacement. Stage 0: catchments draining across the fault zone. Stage 1 (immediately after fault displacement): left-lateral slip generates channel deflections and fault subparallel channels. Offset of ridges and formation of fault-facing facets. Stage 2: growth of new channels from fault subparallel channels results in lateral migration of catchment divides (thick black arrows), thus erasing fault-facing facets and leading to continuous ridges. Stage 3: continuous fault displacement results in lengthening of fault subparallel channels. The growth of new streams leads to the widening of catchments upstream from the fault zone, resulting in asymmetric catchments. Coloured dots illustrate the progressive lengthening of fault subparallel channels.

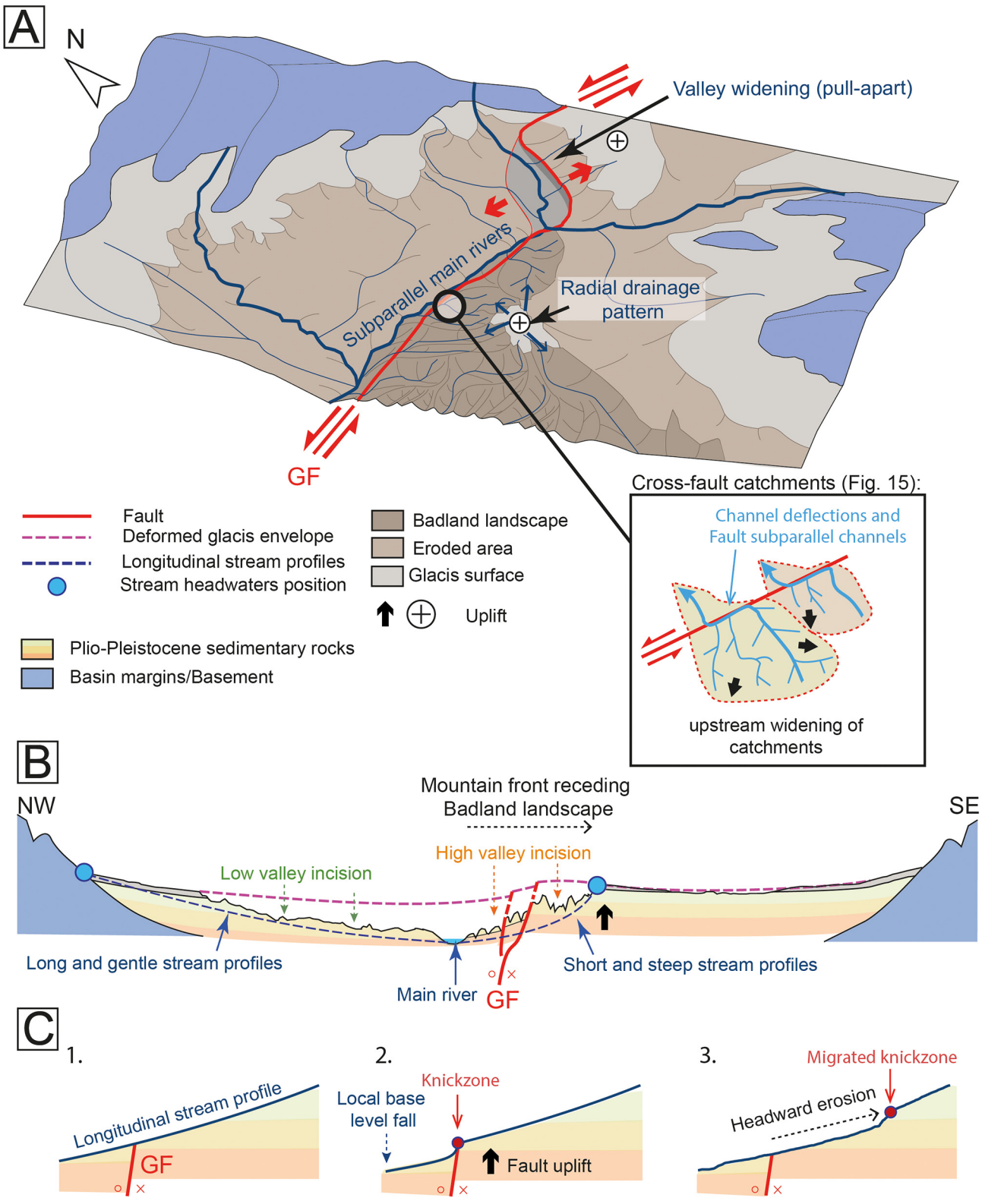

Fig. 16. (A) Schematic sketch (oblique view) and (B) schematic section illustrating the geomorphic effects produced by the horizontal and vertical displacement of the study area. (C) Schematic sketches illustrating the process of upstream knickzone migration observed in longitudinal stream profiles in Fig. 11A. Stage 1: stream in a steady stage. Stage 2: fault uplift and subsequent base-level fall. Knickzone in line with fault trace. Stage 3: headward erosion leads to upstream knickzone migration, reflecting a rapid landscape response.

(Bousquet, 1979), which are responsible for Plio-Quaternary active mountain fronts that characterize the present relief of the SE sector of the cordillera (Fig. 17) (Silva et al., 2003).

In contrast, oblique-slip faults in the central Betic Cordillera (Fig. 17) accommodate WSW-ENE regional extension (e.g., Gil et al., 2002; Galindo-Zaldívar et al., 2015), which has been attributed to back-arc

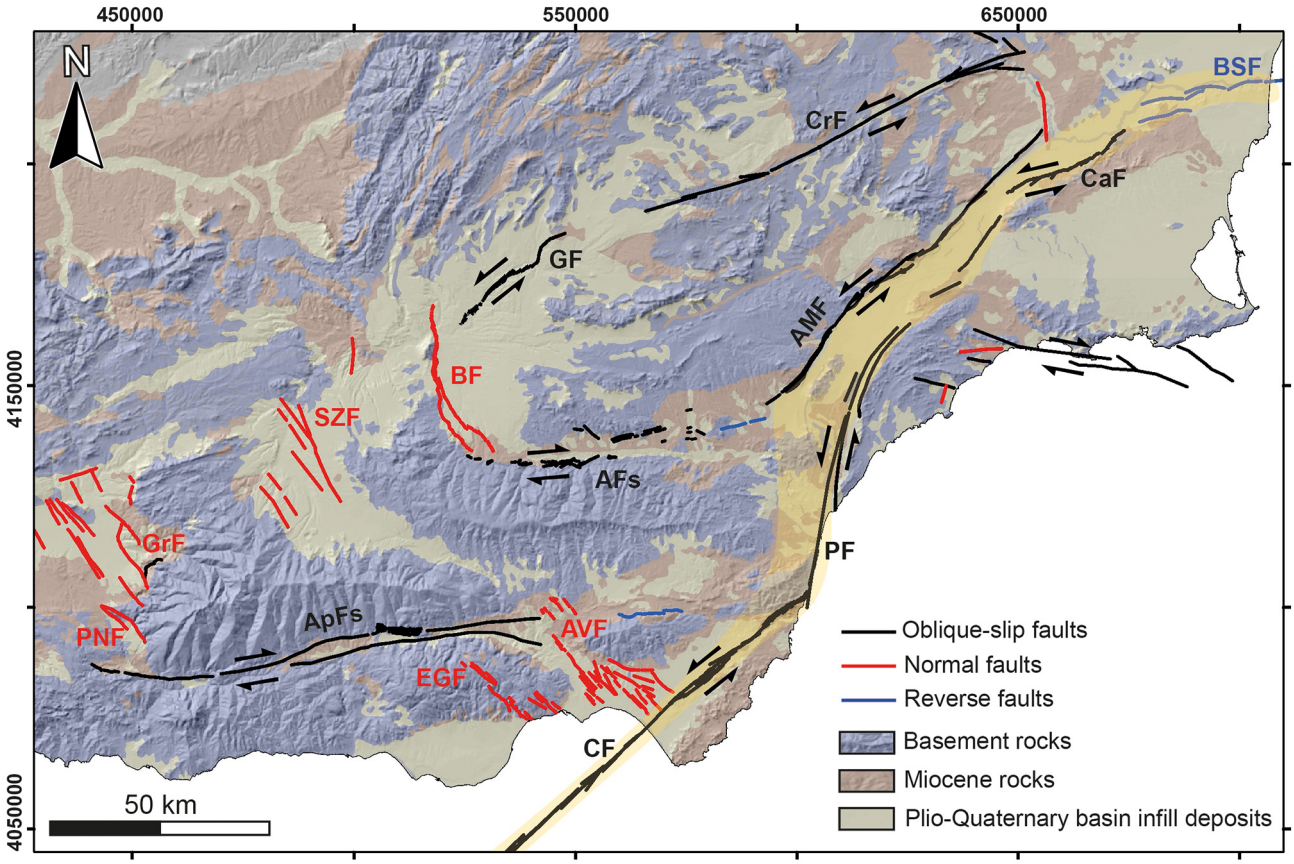

Fig. 17. Map showing the main active faults in the eastern and central Betic Cordillera. The yellow shaded area indicates the Eastern Betic Shear Zone. PNF: Padul-Nigüelas Fault, GrF: Granada Faults, GF: Galera Fault, BF: Baza Fault, AFs: Almanzora Faults, ApFs: Alpujarra Faults, EGF: Eastern Gador Faults, AVF: Andarax Valley Faults, CF: Carboneras Fault, PF: Palomares Fault, AMF: Alhama de Murcia Fault, CaF: Carrascoy Fault, BSF: Bajo Segura Fault, and CrF: Crevillente Fault. Fault traces from the Quaternary Active Faults Database of Iberia (QAFI, García-Mayordomo et al., 2012).

extensional processes (Galindo-Zaldívar et al., 2015) or to lithospheric delamination (e.g., Mancilla et al., 2013). Some of these faults have been defined as transfer structures related to normal faults (Martínez-Martínez et al., 2006; Alfaro et al., 2021). As a result of this regional extension, they present right-lateral and normal kinematics (e.g., the Almanzora and Alpujarra faults, Sanz de Galdeano et al., 1985; Martínez-Martínez et al., 2006; Pedrera et al., 2012). An exception is the GF, which shows left-lateral kinematics with a secondary vertical slip component. Structural and morphometric analyses demonstrate that the Almanzora and Alpujarra faults are active basin-border structures that have contributed, together with folding, to the development of elongated basins (Almanzora and Alpujarra corridors) and the uplift of reliefs in the central Betic Cordillera (Pedrera et al., 2007; Pérez-Peña et al., 2010a).

Both the oblique-slip faults of the eastern and central Betic Cordillera have left, in addition, a well-marked geomorphic imprint on the landscape, given mainly by features such as offset channels and alluvial fans, fault-related knickpoints in longitudinal profiles, drainage network asymmetries, and higher entrenchment of valleys in the uplifted blocks (e.g., Silva et al., 2003; Booth-Rea et al., 2004; Pérez-Peña et al., 2010a; Ferrater et al., 2017; Martin-Banda et al., 2021).

Our structural-morphometric analysis indicates that the tectonic activity of the GF contributed to topographic growth from the Middle Pleistocene onwards, as evidenced by the vertical deformation of the glacis surface (Fig. 9). Similar evidence was described by previous authors for the normal Baza Fault (García-Tortosa et al., 2008b), located to the SW of the GF (Fig. 1), suggesting that relief building continues at present at least in the Baza sub-basin.

However, the impact of the GF in the relief is very low in comparison with the abovementioned oblique-slip structures in the Betic Cordillera. These differences cannot be attributed only to the slow slip rate of the GF (García-Tortosa et al., 2011; Alfaro et al., 2021; and this study), as all the oblique-slip faults in the Betic Cordillera are slow-moving structures, with horizontal slip rates ranging between ~0.5 mm/yr and ~1.5 mm/yr, and uplift rates ranging between ~0.05 and ~0.4 mm/yr (e.g., Braga et al., 2003; Silva et al., 2003; Booth-Rea et al., 2004; Echeverria et al., 2013, 2015; Moreno et al., 2015; Ferrater et al., 2017; Martin-Banda et al., 2021). The intrabasinal nature of the GF is its main difference from other oblique-slip active faults in the Betic Cordillera, in which uplifted blocks are formed mainly by basement rocks (Fig. 17). These basement rocks are much less erodible than the Plio-Pleistocene lacustrine deposits of the Baza sub-basin infill; therefore, they favour the preservation of mountain fronts and other geomorphic effects related to fault displacement. In contrast, the low relief related to the GF, the poor exposure of the fault traces and the rapid erasing of many geomorphic features make this structure difficult to detect. However, in this work, we demonstrate that the control that the GF exerts on the landscape leaves a series of geomorphic anomalies that can be identified by applying a proper morphometric analysis.

7. Conclusions

In the present work, we provide a good example for analysing the tectonic geomorphology of slow-moving, intrabasinal faults and their influence on the evolution of recent Quaternary landscapes. The case study is the Galera Fault (GF) (Guadix-Baza Basin, central Betic

Cordillera, southern Spain), an active oblique-slip fault with a main horizontal component of displacement. Through the study of this fault, we demonstrate the usefulness of integrating geological-structural studies with morphometric analyses. We also prove that geomorphic indices applied traditionally in basin-border faults (such as the AF, Vf, and k_{sn}) can also be applied to intrabasinal faults.

The geological-structural analysis reveals that the SW-NE GF presents lower Pliocene to Middle Pleistocene highly erodible sedimentary rocks on both fault blocks. The surface geometry of the fault reflects its main left-lateral displacement. The main structural feature of this fault is a kilometric-scale, left-releasing fault bend, which is responsible for the development of a pull-apart basin. From stratigraphic markers, we estimate that the GF is responsible for a maximum vertical displacement of ca. 100 m.

The morphometric analysis shows that the geomorphic expression of slow-moving intrabasinal faults can be obscured by a rapid landscape response to tectonic activity, favoured by slow fault slip rates and the high erodibility of the juxtaposed deposits. Hence, some common features that usually define the geomorphic expression of active faults, such as fault-facing facets, offset cross-fault ridges (PRR close to 1), steps in streambeds (k_{sn} knickzones), and the mountain front, may be erased in this type of fault.

In oblique-slip faults, the obscuring of the geomorphic imprint seems to be more effective on landscape effects related to horizontal displacement. In the case of GF, although it has a main left-lateral slip component, the remaining effects reflecting horizontal displacement are scarce and subtle. They include local left stream deflections and fault-subparallel channels, valley widening related to the left-releasing fault bend, and asymmetric catchments due to the widening of the drainage network upstream from the fault.

In contrast, geomorphic effects reflecting vertical fault displacement are better preserved. Despite the minor vertical component of the GF, the uplift of the southern fault block vertically deformed the Middle Pleistocene glacis surface (90 ± 30 m in the central part), controlled the geometry of the main rivers, and triggered lateral migrations of channels in the study area. Fault uplift also generated drainage network differences between fault blocks. The uplifted fault block is characterized by shorter and steeper streams with higher valley incision (lower Vf values), forming a spectacular badland landscape that characterizes this sector of the Guadix-Baza sub-basin.

The vertical deformation of the glacis surface demonstrates that the GF has contributed to relief building in the Betic Cordillera since the Middle Pleistocene. However, when comparing the GF with other equally active oblique-slip faults in the Betic Cordillera, we observe that the impact of intrabasinal faults in mountain building is very low in comparison with basin-border faults. This condition, together with the poor exposure of intrabasinal faults, may make many of these structures undetectable in studies involving structural mapping, seismic hazard assessment, or exploration of resources. In this work, we demonstrate that geomorphological analyses are an essential tool for detecting these structures; although they do not generate significant relief, they exert a control on landscape evolution at different scales.

Declaration of competing interest

The authors declare that they have no known competing financial interests or personal relationships that could have appeared to influence the work reported in this paper.

Acknowledgements

This work was funded by the research project TASCUB (RTI2018-100737-B-I00) of the Spanish Ministry of Science, Innovation and Universities, the research group VIGROB053 (University of Alicante), and the research group RNM 325 of the Junta de Andalucía. Iván Medina Cascales was funded by Ph.D. contract FPU16/00202 of the Spanish Ministry of Science, Innovation and Universities. We would like to thank the editor Martin Stokes, and the reviewers Francisco Moral, Pablo G. Silva, and the anonymous reviewer, whose useful comments and suggestions greatly improved the manuscript.

References

Agustí, J., Martín-Suárez, E., 1984. El Plioceno continental de la depresión Guadix-Baza (Prov. Granada) y su fauna de micromamíferos. Nota preliminar. Acta Geol. Hisp. 19 (4), 277–281.

Alberdi, M.T., Alcalá, L., Azanza, B., Cerdeño, E., Mazo, A.V., Morales, J., Sesé, C., 1989. Consideraciones biostratigráficas sobre la fauna de Vertebrados fósiles de la cuenca de Guadix-Baza (Granada, España). In: Alberdi, M.T., Bonnadonna, F.P. (Eds.), Geología y paleontología de la cuenca de Guadix-Baza. Trabajos sobre el Neógeno Cuaternario11. Museo Nacional de Ciencias Naturales, CSIC, Madrid, pp. 347–355.

Alfaro, P., Delgado, J., Sanz de Galdeano, C., Galindo-Zaldívar, J., García-Tortosa, F.J., López-Garrido, A.C., López-Casado, C., Marín-Lechado, A., Gil, A., Borque, M.J., 2008. The Baza Fault: a major active extensional fault in the central Betic Cordillera (south Spain). Int. J. Earth Sci. 97, 1353–1365. https://doi.org/10.1007/s00531-007-0213-z.

Alfaro, P., Sánchez-Alzola, A., Martin-Rojas, I., García-Tortosa, F.J., Galindo-Zaldívar, J., Avilés, M., López Garrido, A.C., Sanz de Galdeano, C., Ruano, P., Martínez, F., Pedrera, A., Lacy, M.C., Borque, M.J., Medina-Cascales, I., Gil, A.J., 2021. Geodetic fault slip rates on active faults in the Baza sub-basin (SE Spain). Insights for seismic hazard assessment. J. Geodyn. 144, 101815. https://doi.org/10.1016/j.jog.2021.101815.

Allen, C.R., Gillespire, A.R., Han, Y., Sich, K.E., Zhang, B., Zhy, C., 1984. Red River and associated faults, Yunnan Province, China: Quaternary geology, slip rates, and seismic hazard. Geol. Soc. Am. Bull. 95 (6), 686–700. https://doi.org/10.1130/0016-7606(1984)95%3C686:RRAAFY%3E2.0.CO;2.

Arrowsmith, J.R., Zielke, O., 2009. Tectonic geomorphology of the San Andreas Fault zone from high resolution topography: an example from the Cholame segment. Geomorphology 113 (1–2), 70–81. https://doi.org/10.1016/j.geomorph.2009.01.002.

Barth, N.C., 2013. A Tectono-Geomorphic Study of the Alpine Fault, New Zealand. (PhD Thesis)University of Otago (319 pp.).

Bellin, N., Vanacker, V., Kubik, P.W., 2014. Denudation rates and tectonic geomorphology of the Spanish Betic Cordillera. Earth Planet. Sci. Lett. 390, 19–30. https://doi.org/10.1016/j.epsl.2013.12.045.

Bishop, P., 2007. Long-term landscape evolution: linking tectonics and surface processes. Earth Surf. Process. Landf. 32, 329–365. https://doi.org/10.1002/esp.1493.

Boncio, P., Lavecchia, G., Pace, B., 2004. Defining a model of 3D seismogenic sources for Seismic Hazard Assessment applications: the case of central Apennines (Italy). J. Seismol. 8, 407–425. https://doi.org/10.1023/B:JOSE.0000038449.78801.05.

Booth-Rea, G., Azañón, J.M., Azor, A., García-Dueñas, V., 2004. Influence of strike-slip fault segmentation on drainage evolution and topography. A case study: the Palomares Fault Zone (southeastern Betics, Spain). J. Struct. Geol. 26 (9), 1615–1632. https://doi.org/10.1016/j.jsg.2004.01.007.

Borque, M., Sanchez-Alzola, A., Martin-Rojas, I., Alfaro, P., Molina, S., Rosa-Cintas, S., Rodríguez-Caderot, G., Lacy, C., García-Armenteros, J., Avil'es, M., Herrera-Olmo, A., García-Tortosa, F., Est'evez, A., Gil, A.J., 2019. How much nubia-eurasia convergence is accommodated by the NE end of the eastern betic shear zone (SE Spain)? Constraints from GPS velocities. Tectonics 38, 1824–1839. https://doi.org/10.1029/2018TC004970.

Boulton, S.J., Whittaker, A.C., 2009. Quantifying the slip rates, spatial distribution and evolution of active normal faults from geomorphic analysis: field examples from an oblique-extensional graben, southern Turkey. Geomorphology 104, 299–316. https://doi.org/10.1016/j.geomorph.2008.09.007.

Bousquet, J.C., 1979. Quaternary strike-slip faults in southeastern Spain. Tectonophysics 52 (1–4), 277–286. https://doi.org/10.1016/0040-1951(79)90232-4.

Braga, J.C., Martín, J.M., Quesada, C., 2003. Patterns and average rates of late Neogene–recent uplift of the Betic Cordillera, SE Spain. Geomorphology 50 (1–3), 3–26. https://doi.org/10.1016/S0169-555X(02)00205-2.

Bull, W.B., 1977. Tectonic geomorphology of the Mojave Desert, California. USGS Contract Report 14-0-001-G-394. Office of Earthquakes, Volcanoes, and Engineering, Menlo Park, California 1977. (188 pp).

Bull, W.B., 2007. Tectonic Geomorphology of Mountains: A New Approach to Paleosiesmology. Blackwell publishing, Oxford, U.K. (320 pp).

Bull, W.B., 2009. Geomorphic Responses to Climatic Change. Blackburn Press, New Jersey (326 pp.).

Bull, W.B., McFadden, L., 1977. Tectonic geomorphology North and South of the Garlock fault, California. In: Dohering, D.O. (Ed.), Geomorphology in Arid Regions. Publ. in Geomorphology. State University of New York, Binghamton, pp. 115–138.

Burbank, D.W., Anderson, R.S., 2013. Tectonic Geomorphology. 2nd edition. Wiley-Blackwell (454 pp).

Calvache, M.L., Viseras, C., 1995. Consecuencias geomorfológicas derivadas de un proceso de captura fluvial. Geogaceta 18, 93–96.

Calvache, M.L., Viseras, C., 1997. Long-term control mechanisms of stream piracy processes in southeastern Spain. Earth Surf. Process. Landf. 22, 93–105.

Castillo, M., Muñoz-Salinas, E., Ferrari, L., 2014. Response of a landscape to tectonics using channel steepness indices (k_{sn}) and OSL: a case of study from the Jalisco Block, Western Mexico. Geomorphology 221, 204–214. https://doi.org/10.1016/j.geomorph.2014.06.017.

Centro Nacional de Información Geográfica, d. Downloads Centre. https://centrodedescargas.cnig.es/CentroDescargas/index.jsp. (Accessed 25 October 2020).

Chartier, T., Scotti, O., Lyon-Caen, H., 2019. SHERIFS: open-source code for computing earthquake rates in fault systems and constructing hazard models. Seismol. Res. Lett. 90 (4), 1678–1688. https://doi.org/10.1785/0220180332.
Chevalier, M.L., Leloup, P.H., Replumaz, A., Pan, J., Liu, D., Li, H., Gourbet, L., Métois, M., 2016. Tectonic-geomorphology of the Litang fault system, SE Tibetan Plateau, and implication for regional seismic hazard. Tectonophysics 682, 278–292. https://doi.org/10.1016/j.tecto.2016.05.039.
Coppier, G., Griveaud, P., de Larouziere, F.D., Montenat, C., Ott d'Estevou, P., 1989. Example of Neogene tectonic indentation in the Eastern Betic Cordilleras: the Arc of Aguilas (Southeastern Spain). Geodin. Acta 3 (1), 37–51. https://doi.org/10.1080/09853111.1989.11105173.
Crosetto, S., Watkinson, I.M., Min, S., Gori, S., Falcucci, E., Le Ngal, N., 2018. Evidence of Quaternary and recent activity along the Kyaukkyan Fault, Myanmar. J. Asian Earth Sci. 156, 207–225. https://doi.org/10.1016/j.jseaes.2018.01.013.
Davis, W.M., 1903. The mountain ranges of the Great Basin. Bull. Mus. Comp. Zool. 42, 129–177.
De Larouzière, F.D., Bolze, J., Bordet, P., Hernández, J., Montenat, C., Ott d'Estevou, P., 1988. The Betic segment of the lithospheric Trans-Alboran shear zone during the Late Miocene. Tectonophysics 152 (1–2), 41–52. https://doi.org/10.1016/0040-1951(88)90028-5.
DeMets, C., Gordon, R.G., Argus, D.F., 2010. Geologically current plate motions. Geophys. J. Int. 181 (1), 1–80. https://doi.org/10.1111/j.1365-246X.2009.04491.x.
Demoulin, A., 1998. Testing the tectonic significance of some parameters of longitudinal river profiles: the case of the Ardenne (Belgium, NW Europe). Geomorphology 24, 189–208. https://doi.org/10.1016/S0169-555X(98)00016-6.
Demoulin, A., 2011. Basin and river profile morphometry: a new index with a high potential for relative dating of tectonic uplift. Geomorphology 126, 97–107. https://doi.org/10.1016/j.geomorph.2010.10.033.
Dhanya, V., Tiruvanatpuram, K., 2014. Basin asymmetry and associated tectonics: a case study of Achankovil river basin, Kerala. Transactions 36, 207–215.
Díaz-Hernández, J.L., Juliá, R., 2006. Geochronological position of badlands and geomorphological patterns in the Guadix-Baza basin (SE Spain). Quat. Res. 65, 467–477. https://doi.org/10.1016/j.yqres.2006.01.009.
Dumas, B., 1969. Glacis et croutes calcaires dans le Levant espagnole. Bull. Assoc. Géogr. Fr. 46, 553–561. https://doi.org/10.3406/bagf.1969.5928.
Duvall, A.R., Tucker, G.E., 2015. Dynamic ridges and valleys in a strike-slip environment. J. Geophys. Res. Earth Surf. 120 (10), 2016–2026. https://doi.org/10.1002/2015JF003618.
Echeverria, A., Khazaradze, G., Asensio, E., Gárate, J., Dávila, J.M., Suriñach, E., 2013. Crustal deformation in eastern Betics from CuaTeNeo GPS network. Tectonophysics 608, 600–612. https://doi.org/10.1016/j.tecto.2013.08.020.
Echeverria, A., Khazaradze, G., Asensio, E., Masana, E., 2015. Geodetic evidence for continuing tectonic activity of the Carboneras fault (SE Spain). Tectonophysics 663, 302–309. https://doi.org/10.1016/j.tecto.2015.08.009.
El Hamdouni, R., Irigaray, C., Fernández, T., Chacón, J., Keller, E.A., 2008. Assessment of relative active tectonics, southwest border of the Sierra Nevada (southern Spain). Geomorphology 96, 150–173. https://doi.org/10.1016/j.geomorph.2007.08.004.
Eusden, J.D., Pettinga, J.R., Campbell, J.C., 2000. Structural evolution and landscape development of a collapsed transpressive duplex on the Hope Fault, North Canterbury, New Zealand. New Zealand J. Geol. Geophys. 43, 391–404. https://doi.org/10.1080/00288306.2000.9514896.
Farines, B., Calvet, M., Gunnell, Y., 2015. The summit erosion surfaces of the inner Betic Cordillera: their value as tools for reconstructing the chronology of topographic growth in southern Spain. Geomorphology 233, 92–111. https://doi.org/10.1016/j.geomorph.2014.11.019.
Ferrater, M., Ortuño, M., Masana, E., Martínez-Díaz, J.J., Pallàs, R., Perea, H., Baize, E., Garcia-Meléndez, E., Echeverria, A., Rockwell, T., Sharp, W.D., Arrosmith, R., 2017. Lateral slip rate of Alhama de Murcia fault (SE Iberian Peninsula) based on a morphotectonic analysis: comparison with paleoseismological data. Quat. Int. 451, 87–100. https://doi.org/10.1016/j.quaint.2017.02.018.
Field, E.H., Biasi, G.P., Bird, P., Dawson, T.E., Felzer, K.R., Jackson, D.D., Johnson, K.M., Jordan, T.H., Madden, C., Michael, A.J., Milner, K.R., Page, M.T., Parsons, T., Powers, P. M., Shaw, B.E., Thatcher, W.R., Weldon, R.J., Zeng, Y., 2015. Long-term time-dependent probabilities for the third Uniform California Earthquake Rupture Forecast (UCERF3). BSSA 105 (2A), 511–543. https://doi.org/10.1785/0120140093.
Flint, J.J., 1974. Stream gradient as a function of order magnitude and discharge. Water Resour. Res. 10, 969–973. https://doi.org/10.1029/WR010i005p00969.
Freudenthal, M., Mein, P., Martín-Suárez, E., 1998. Revision of Late Miocene and Pliocene Cricetinae (Rodentia, Mammalia) from Spain and France. Treb. Mus. Geol. Barcelona 7, 11–93.
Galindo-Zaldívar, J., González-Lodeiro, F., Jabaloy, A., 1993. Stress and palaeostress in the Betic-Rif cordilleras (Miocene to the present). Tectonophysics 227 (1–4), 105–126. https://doi.org/10.1016/0040-1951(93)90090-7.
Galindo-Zaldívar, J., Jabaloy, A., Serrano, I., Morales, J., González-Lodeiro, F., Torcal, F., 1999. Recent and present-day stresses in the Granada Basin (Betic Cordilleras): example of a late Miocene-present-day extensional basin in a convergent plate boundary. Tectonics 18 (4), 686–702. https://doi.org/10.1029/1999TC900016.
Galindo-Zaldívar, J., Gil, A.J., Sanz de Galdeano, C., Lacy, M.C., García-Armenteros, J.A., Ruano, P., Ruiz, A.M., Martínez-Martos, M., Alfaro, P., 2015. Active shallow extension in central and eastern Betic Cordillera from CGPS data. Tectonophysics 663, 290–301. https://doi.org/10.1016/j.tecto.2015.08.035.
Garcés, M., Agustí, J., Parés, J.M., 1997. Late Pliocene continental magnetochronology in the Guadix-Baza Basin (Betic Ranges, Spain). Earth Planet. Sci. Lett. 146, 677–687. https://doi.org/10.1016/S0012-821X(96)00240-3.
García-Aguilar, J.M., Martín, J.M., 2000. Late Neogene to recent continental history and evolution of the Guadix-Baza basin (SE Spain). Rev. Soc. Geol. Esp. 13 (1), 65–77.
García-Aguilar, J.M., Palmqvist, P., 2011. A model of lacustrine sedimentation for the Early Pleistocene deposits of Guadix-Baza basin (southeast Spain). Quat. Int. 243 (1), 3–15. https://doi.org/10.1016/j.quaint.2011.02.008.
García-Delgado, H., Velandia, F., 2020. Tectonic geomorphology of the Serranía de San Lucas (Central Cordillera): regional implications for active tectonics and drainage rearrangement in the Northern Andes. Geomorphology 349. https://doi.org/10.1016/j.geomorph.2019.106914.
García-Mayordomo, J., Insua-Arévalo, J.M., Martínez-Díaz, J.J., Jiménez-Díaz, A., Martín-Banda, R., Martín-Alfageme, S., Álvarez-Gómez, J.A., Rodríguez-Peces, M., Pérez-López, R., Rodríguez-Pascua, M.A., Masana, E., Perea, H., Martín-González, F., Giner-Robles, J., Nemser, E.S., Cabral, J., the QAFI Compilers Working Group, 2012. The quaternary faults database of Iberia (QAFI v.2.0). J. Iber. Geol. 38 (1), 285–302.
García-Tortosa, F.J., Sanz de Galdeano, C., Alfaro, P., Galindo-Zaldívar, J., Peláez, J.A., 2007. La falla y los pliegues de Galera. In: Sanz de Galdeano, C., Peláez, J.A. (Eds.), La cuenca de Guadix-Baza: estructura, tectónica activa, sismicidad, geomorfología y dataciones existentes. Universidad de Granada, pp. 141–153.
García-Tortosa, F.J., Sanz de Galdeano, C., Alfaro, P., Jiménez Espinosa, R., Jiménez-Millán, J., Lorite Herrera, M., 2008a. Nueva evidencia sobre la edad del tránsito endorreico-exorreico de la cuenca de Guadix-Baza. Geogaceta 44, 211–214.
García-Tortosa, F.J., Alfaro, P., Galindo Zaldívar, J., Gibert, L., López Garrido, A.C., Sanz de Galdeano, C., Ureña, M., 2008b. Geomorphologic evidence of the active Baza fault (Betic Cordillera, South Spain). Geomorphology 97 (3–4), 374–391. https://doi.org/10.1016/j.geomorph.2007.08.007.
García-Tortosa, F.J., Alfaro, P., Galindo, Zaldívar J., Sanz de Galdeano, C., 2011. Glacis geometry as a geomorphic marker of recent tectonics: the Guadix-Baza Basin (South Spain). Geomorphology 125 (4), 517–529. https://doi.org/10.1016/j.geomorph.2010.10.021.
Gibert, L., Scott, G., Ferràndez-Canyadell, C., 2006. Evaluation of the Olduvai sub-chron in the Orce Ravine (SE Spain). Implications for Plio-Pleistocene mammal biostratigraphy and the age of Orce archaeological sites. Quat. Sci. Rev. 25, 507–525. https://doi.org/10.1016/j.quascirev.2005.03.006.
Gibert, L., Ortí, F., Rosell, L., 2007a. Plio-Pleistocene lacustrine evaporites of the Baza Basin (Betic Chain, SE Spain). Sediment. Geol. 200 (1–2), 89–116. https://doi.org/10.1016/j.sedgeo.2007.03.003.
Gibert, L., Scott, G., Martin, R., Gibert, J., 2007b. The Early to Middle Pleistocene boundary in the Baza Basin (Spain). Quat. Sci. Rev. 26 (17–18), 2067–2089. https://doi.org/10.1016/j.quascirev.2007.06.012.
Gil, A.J., Rodríguez-Caderot, G., Lacy, M.C., Ruiz, A.M., Sanz de Galdeano, C., Alfaro, P., 2002. Establishment of a Non-Permanent GPS Network to Monitor the Recent NE-SW Deformation in the Granada Basin (Betic Cordillera, Southern Spain). First results from a non-permanent GPS network. Stud. Geophys. Geod. 46, 395–409. https://doi.org/10.1023/A:1019530716324.
Guerra-Merchán, A., 1992. Origen y relleno sedimentario de la cuenca neógena del corredor del Almanzora y áreas limítrofes (Cordillera Bética). (PhD Thesis) Universidad de Granada, Spain (237 pp.).
Gürbüz, E., Kazanci, N., Gürbüz, A., 2015. Strike–slip faulting, topographic growth and block movements as deduced from drainage anomalies: the Yeşilırmak River basin, northern Turkey. Geomorphology 246, 634–648. https://doi.org/10.1016/j.geomorph.2015.07.018.
Haberland, C., Gibert, L., José Jurado, M., Stiller, M., Baumann-Wilke, M., Scott, G., Mertz, D. F., 2017. Architecture and tectono-stratigraphic evolution of the intramontane Baza Basin (Bétics, SE-Spain): constraints from seismic imaging. Tectonophysics 709, 69–84. https://doi.org/10.1016/j.tecto.2017.03.022.
Hack, J.T., 1973. Stream-profiles analysis and stream-gradient index. J. Res. U.S. Geol. Survey 1 (4), 421–429.
Hare, P.W., Gardner, T.W., 1985. Geomorphic indicators of vertical neotectonism along converging plate margins, Nicoya Peninsula, Costa Rica. In: Morisawa, M., Hack, J.T. (Eds.), Tectonic Geomorphology. Proceedings of the 15th Annual Bighamton Geomorphology Symposium. Allen & Unwin, Boston, pp. 75–104.
Herraiz, M., De Vicente, G., Lindo-Ñaupari, R., Giner, J., Simón, J.L., González-Casado, J.M., Vadillo, O., Rodríguez-Pascua, M.A., Cicuéndez, J.I., Casas, A., Cabañas, L., Rincón, P., Cortés, A.L., Ramírez, M., Lucini, M., 2000. The recent (upper Miocene to Quaternary) and present tectonic stress distributions in the Iberian Peninsula. Tectonics 19, 762–786. https://doi.org/10.1029/2000TC900006.
Hovius, N., 2000. Macroscale process systems of mountain belt erosion. In: Summerfield, M.A. (Ed.), Geomorphology and Global Tectonics. Whiley and Sons, Chichester, pp. 77–105.
Huang, L., Liu, C., Wang, Y., Xue, Y., Zhao, J., 2016. Hydrocarbon accumulation in strike-slip fault restraining bends: New insights into the tectonic controls on the Penglai 19-3 and Penglai 25-6 oil fields, Tan-Lu fault zone, east China. AAPG Bull. 100 (8), 1239–1263. https://doi.org/10.1306/03041614086.
Jackson, J., Norris, R., Youngson, J., 1996. The structural evolution of active fault and fold systems in central Otago, New Zealand: evidence revealed by drainage patterns. J. Struct. Geol. 18, 217–234. https://doi.org/10.1016/S0191-8141(96)80046-0.
Johnson, S.Y., Watt, J.T., 2012. Influence of fault trend, bends, and convergence on shallow structure and geomorphology of the Hosgri strike-slip fault, offshore central California. Geosphere 8, 1632–1656. https://doi.org/10.1130/GES00830.1.
Joshi, N., Kothyari, G.C., Pant, C.C., 2021. Drainage conformation and transient response of river system in thrust segmentation of Northwest Himachal Himalaya, India. Quat. Int. 575–576, 37–50. https://doi.org/10.1016/j.quaint.2020.05.024.
Keller, E.A., Pinter, N., 1996. Active Tectonics. Prentice-Hall, Upper Saddle River (338 pp.).
Keller, E.A., Pinter, N., 2002. Active Tectonics: Earthquakes, Uplift and Landscape. 2nd ed. Prentice-Hall, Upper Saddle River (362 pp.).
Kirby, E., Whipple, K.X., 2012. Expression of active tectonics in erosional landscapes. J. Struct. Geol. 44, 54–75. https://doi.org/10.1016/j.jsg.2012.07.009.

Litchfield, N.J., 2001. The Titri Fault System: Quaternary-active faults near the leading edge of the Otago reverse fault province. New Zealand J. Geol. Geophys. 44, 517–534. https://doi.org/10.1080/00288306.2001.9514953.

Liu, L., Chen, H., Zhong, Y., Wang, J., Du, X., Zou, H., 2021. Depositional architectures and sedimentation processes in strike-slip extensional basins: examples from the Oligocene of the Liaodong Bay Sub-basin, Bohai Bay Basin, China. Mar. Pet. Geol. 123, 104788. https://doi.org/10.1016/j.marpetgeo.2020.104788.

Maldonado-Garrido, E., Pinero, P., Agusti, J., 2017. A catalogue of the vertebrate fossil record from the Guadix-Baza Basin (SE Spain). Span. J. Palaeontol. 32 (1), 207–236.

Mancilla, F.L., Stich, D., Berrocoso, M., Martin, R., Morales, J., Fernandez-Ros, A., Paez, R., Perez-Pena, A., 2013. Delamination in the Betic Range: deep structure, seismicity, and GPS motion. Geology 41 (3), 307–310. https://doi.org/10.1093/gji/ggu214.

Mann, P., Hempton, M.R., Bradley, D.C., Burke, K., 1983. Development of pull-apart basins. J. Geol. 91 (5), 529–554.

Marliyani, G.I., Arrowsmith, J.R., Whipple, K.X., 2016. Characterization of slow slip rate faults in humid areas: Cimandiri fault zone, Indonesia. J. Geophys. Res. Earth Surf. 121, 2287–2308. https://doi.org/10.1002/2016JF003846.

Martin-Banda, R., García-Mayordomo, J., Insua-Arévalo, J.M., Salazar, A.E., Rodríguez-Escudero, E., Álvarez-Gómez, J.A., Medialdea, A., Herrero, M.J., 2016. New insights on the seismogenic potential of the Eastern Betic Shear Zone (SE Iberia): Quaternary activity and paleoseismicity of the SW segment of the Carrascoy Fault Zone. Tectonics 35 (1), 55–75. https://doi.org/10.1002/2015TC003997.

Martin-Banda, R., Insua-Arévalo, J.M., García-Mayordomo, J., 2021. Slip rate variation during the last ~210 ka on a slow fault in a transpressive regime: the Carrascoy Fault (Eastern Betic Shear Zone, SE Spain). Front. Earth Sci. 8, 599608. https://doi.org/10.3389/feart.2020.599608.

Martínez-Díaz, J.J., Masana, E., Ortuño, M., 2012. Active tectonics of the Alhama de Murcia fault, Betic Cordillera, Spain. J. Iber. Geol. 38 (1), 253–270. https://doi.org/10.5209/rev_JIGE.2012.v38.n1.39218.

Martínez-Martínez, J.M., Booth-Rea, G., Azañón, J.M., Torcal, F., 2006. Active transfer fault zone linking a segmented extensional system (Betics, southern Spain): insight into heterogeneous extension driven by edge delamination. Tectonophysics 422 (1–4), 159–173. https://doi.org/10.1016/j.tecto.2006.06.001.

Martínez-Solares, J.M., Mezcua, J., 2002. Catálogo sísmico de la Península Ibérica (880 AC-1900). Monografía n° 18. Instituto Geográfico Nacional, Madrid, Spain (254 pp.).

Martín-Suárez, E., 1988. Sucesiones de micromamíferos en la Depresión de Guadix-Baza (Granada, España). (PhD Thesis (unpublished))Univiversidad de Granada, Granada (241 pp.).

Massironi, M., Kim, Y.S., 2015. Strike-slip faults. In: Hargitai, H., Kereszturi, Á. (Eds.), Encyclopedia of Planetary Landforms. Springer, New York, NY. https://doi.org/10.1007/978-1-4614-3134-3_548.

Matoš, B., Pérez-Peña, J.V., Tomljenović, B., 2016. Landscape response to recent tectonic deformation in the SW Pannonian Basin: evidence from DEM-based morphometric analysis of the Bilogora Mt. area, NE Croatia. Geomorphology 263, 132–155. https://doi.org/10.1016/j.geomorph.2016.03.020.

Medina-Cascales, I., Martin-Rojas, I., García-Tortosa, F.J., Peláez, J.A., Alfaro, P., 2020. Geometry and kinematics of the Baza Fault (central Betic Cordillera, South Spain): insights into its seismic potential. Geol. Acta 18, 1–25. https://doi.org/10.1344/GeologicaActa2020.18.11.

Mériaux, A.S., Tapponnier, P., Ryerson, F.J., Xiwei, X., King, G., Van der Woerd, J., Finkel, C., Haibing, L., Caffee, M.W., Zhiqin, X., Wenbin, C., 2005. The Aksay segment of the northern Altyn Tagh fault: tectonic geomorphology, landscape evolution, and Holocene slip rate. J. Geophys. Res. Solid Earth 110, B04404. https://doi.org/10.1029/2004JB003210.

Molin, P., Pazzaglia, F.J., Dramis, F., 2004. Geomorphic expression of active tectonics in a rapidly-deforming forearc, Sila Massif, Calabria, southern Italy. Am. J. Sci. 304 (7), 559–589. https://doi.org/10.2475/ajs.304.7.559.

Moral, F., Balanyá, J.C., 2020. Recent fault-controlled glacis deformation and its role in the fluvial capture of the Guadix-Baza basin (Betic Cordillera, southern Spain). Geomorphology 363. https://doi.org/10.1016/j.geomorph.2020.107226.

Moreno, X., Masana, E., Pallàs, R., Gràcia, E., Rodés, A., Bordonau, J., 2015. Quaternary tectonic activity of the Carboneras Fault in the La Serrata range (SE Iberia): geomorphological and chronological constraints. Tectonophysics 663, 78–94. https://doi.org/10.1016/j.tecto.2015.08.016.

Mukhopadhyay, A., Chaudhuri, P.N., Banerji, A.L., 1984. Contemporaneous intrabasinal faulting in Gondawana Basin - the Jurabaga fault of IB River Coalfield, a type example. J. Geol. Soc. India 25 (9), 557–563.

Nicol, A., Van Dissen, R., 2002. Up-dip partitioning of displacement components on the oblique-slip Clarence Fault, New Zealand. J. Struct. Geol. 24, 1521–1534. https://doi.org/10.1016/S0191-8141(01)00141-9.

Nocquet, J.M., 2012. Present-day kinematics of the Mediterranean: a comprehensive overview of GPS results. Tectonophysics 579, 220–242. https://doi.org/10.1016/j.tecto.2012.03.037.

Ollier, C.C., 1981. Tectonics and Landforms. Longman, New York (324 pp.).

Oms, O., Agustí, J., Gabà, M., Anadó, P., 2000. Lithostratigraphical correlation of micromammal sites and biostratigraphy of the Upper Pliocene to Lower Pleistocene in the Northeast Guadix-Baza Basin (southern Spain). J. Quat. Sci. 15 (1), 43–50. https://doi.org/10.1002/(SICI)1099-1417(200001)15:1%3C43::AID-JQS475%3E3.0.CO;2-9.

Oms, O., Anadón, P., Agustí, J., Julià, R., 2011. Geology and chronology of the continental Pleistocene archeological and paleontological sites of the Orce area (Baza basin, Spain). Quat. Int. 243, 33–43. https://doi.org/10.1016/j.quaint.2011.03.048.

Özsayin, E., 2016. Relative tectonic activity assessment of the Çameli Basin, Western Anatolia, using geomorphic indices. Geodin. Acta 28, 241–253. https://doi.org/10.1080/09853111.2015.1128180.

Pain, C.F., 1985. Cordilleran metamorphic core complexes in Arizona: a contribution from geomorphology. Geology 13 (12), 871–874. https://doi.org/10.1130/0091-7613(1985)13%3C871:CMCCIA%3E2.0.CO;2.

Palano, M., González, P.J., Fernández, J., 2015. The diffuse plate boundary of Nubia and Iberia in the Western Mediterranean: crustal deformation evidence for viscous coupling and fragmented lithosphere. Earth Planet. Sci. Lett. 430, 439–447. https://doi.org/10.1016/j.epsl.2015.08.040.

Patria, A., Putra, P.S., 2020. Development of the Palu–Koro Fault in NW Palu Valley, Indonesia. Geosci. Lett. 7, 1. https://doi.org/10.1186/s40562-020-0150-2.

Pedrera, A., 2008. Structure and tectonic evolution of the Almanzora corridor and the western Huércal-Overa basin (Eastern Betic Cordillera). (PhD Thesis)Universidad de Granada (201 pp.).

Pedrera, A., Galindo-Zaldívar, J., Sanz de Galdeano, C., López-Garrido, A.C., 2006. Superposición de fallas y paleoesfuerzos en el Corredor del Almanzora desde el Tortoniense a la actualidad (Cordilleras Béticas). Geogaceta 39, 59–62.

Pedrera, A., Galindo-Zaldívar, J., Sanz de Galdeano, C., López-Garrido, A.C., 2007. Fold and fault interactions during the development of an elongated narrow basin: the Almanzora Neogene-Quaternary Corridor (SE Betic Cordillera, Spain). Tectonics 26 (6), TC6002. https://doi.org/10.1029/2007TC002138.

Pedrera, A., Galindo-Zaldívar, J., Marín-Lechado, C., García-Tortosa, F.J., Ruano, P., López Garrido, A.C., Azañón, J.M., Peláez, J.A., Giaconia, F., 2012. Recent and active faults and folds in the central-eastern Internal Zones of the Betic Cordillera. J. Iber. Geol. 38 (1), 191–208. https://doi.org/10.5209/rev_JIGE.2012.v38.n1.39213.

Peña, J., 1979. La depresión de Guadix–Baza: Estratigrafía del Plioceno–Pleistoceno. (PhD Thesis)Universidad de Granada (179 pp.).

Peña, J.A., 1985. La depresión de Guadix-Baza. Estud. Geol. 41 (1–2), 33–46. https://doi.org/10.3989/egeol.85411-2688.

Pérez-Peña, J.A., Azañón, J.M., Azor, A., Tuccimei, P., Della Seta, M., Soligo, M., 2009. Quaternary landscape evolution and erosion rates for an intramontane Neogene basin (Guadix–Baza basin, SE Spain). Geomorphology 106, 206–218. https://doi.org/10.1016/j.geomorph.2008.10.018.

Pérez-Peña, J.V., Azor, A., Azañón, J.M., Keller, E.A., 2010a. Active tectonics in the Sierra Nevada (Betic Cordillera, SE Spain): Insights from geomorphic indexes and drainage pattern analysis. Geomorphology 119, 74–87. https://doi.org/10.1016/j.geomorph.2010.02.020.

Pérez-Peña, A., Martín-Dávila, J., Gárate, J., Berrocoso, M., Buforn, E., 2010b. Velocity field and tectonic strain in Southern Spain and surrounding areas derived from GPS episodic measurements. J. Geodyn. 49, 232–240. https://doi.org/10.1016/j.jog.2010.01.015.

Piñero, P., Agustí, J., 2020. Rodents from Botardo-D and the Miocene-Pliocene transition in the Guadix-Baza Basin (Granada, Spain). Paleobiodivers. Paleoenviron. 100, 903–920. https://doi.org/10.1007/s12549-019-00412-4.

Riedel, W., 1929. Zur Mechanik geologischer Brucherscheinungen. Centralblatt Mineral. Abteilung B 354–368.

Ruszkiczay-Rüdiger, Z., Fodor, L.I., Erzsébet, H., 2007. Neotectonics and Quaternary landscape evolution of the Gödöllő Hills, Central Pannonian Basin, Hungary. Glob. Planet. Change 58 (1–4), 181–196. https://doi.org/10.1016/j.gloplacha.2007.02.010.

Ruszkiczay-Rüdiger, Z., Fodor, L.I., Horváth, E., Telbisz, T., 2009. Discrimination of luvial, eolian and neotectonic features in a low hilly landscape: a DEM-based morphotectonic analysis in the Central Pannonian Basin, Hungary. Geomorphology 104, 203–217. https://doi.org/10.1016/j.geomorph.2008.08.014.

Salisbury, J.B., Arrowsmith, J.R., Brown, N., Rockwell, T., Akciz, S., Ludwig, L.G., 2018. The age and origin of small offsets at VanMatre Ranch along the San Andreas fault in the Carrizo Plain, California. Bull. Seismol. Soc. Am. 108, 639–653. https://doi.org/10.1785/0120170162.

Sanz de Galdeano, C., Alfaro, P., 2004. Tectonic significance of the present relief of the Betic Cordillera. Geomorphology 63 (3–4), 175–190. https://doi.org/10.1016/j.geomorph.2004.04.002.

Sanz de Galdeano, C., Vera, J.A., 1992. Stratigraphic record and palaeogeographical context of the Neogene basins in the Betic Cordillera, Spain. Basin Res. 4, 21–36.

Sanz de Galdeano, C., Rodríguez-Fernández, J., López-Garrido, A.C., 1985. A strike-slip fault corridor within the Alpujarra Mountains (Betic Cordilleras, Spain). Geol. Rundsch. 74, 641–655. https://doi.org/10.1007/BF01821218.

Sanz de Galdeano, C., García-Tortosa, F.J., Peláez, J.A., Alfaro, P., Azañón, J.M., Galindo-Zaldívar, J., López-Casado, C., López-Garrido, A.C., Rodríguez-Fernández, J., Ruano, P., 2012. Main active faults in the Granada and Guadix-Baza Basins (Betic Cordillera). J. Iber. Geol. 38 (1), 209–223. https://doi.org/10.5209/rev_JIGE.2012.v38.n1.39215.

Sanz de Galdeano, C., Azañón, J.M., Ruano, P., García-Mayordomo, J., Masana, E., Alfaro, P., Ferrater, M., García-Tortosa, F.J., Gràcia, E., Insua Arévalo, M., Jiménez Bonilla, A., Marín-Lechado, C., Martín Banda, R., Martínez-Díaz, J.J., Martín-Rojas, I., Pedrera, A., 2020. Active faults in the Betic Cordillera. In: Oliveira, J.T., Quesada, C. (Eds.), The Geology of Iberia: A Geodynamic Approach. 5. Springer International Publishing, pp. 56–65.

Schlische, R.W., 1992. Structural and stratigraphic development of the Newark extensional basin, eastern North America: evidence for the growth of the basin and its bounding structures. Geol. Soc. Am. Bull. 104 (10), 1246–1263. https://doi.org/10.1130/0016-7606(1992)104%3C1246:SASDOT%3E2.3.CO;2.

Schumm, S.A., Dumont, J.F., Holbrook, J.M., 2000. Active Tectonics and Alluvial Rivers. Cambridge University Press, Cambridge (276 pp.).

Scott, G., Gibert, L., 2009. The oldest hand-axes in Europe. Nature 461, 82–85. https://doi.org/10.1038/nature08214.

Serpelloni, E., Vannucci, G., Pondrelli, S., Argnani, A., Casula, G., Anzidei, M., Balde, P., Gasperini, P., 2007. Kinematics of the Western Africa-Eurasia plate boundary from focal mechanisms and GPS data. Geophys. J. Int. 169, 1180–1200. https://doi.org/10.1111/j.1365-246X.2007.03367.x.

Sibson, R.H., 1986. Rupture interaction with fault jogs. In: Das, S., Boatwright, J. (Eds.), Earthquake Source Mechanics. AGU Monograph37, pp. 157–167.

Silva Barroso, P.G., Rodríguez Pascua, M.A., Giner Robles, J.L., Pérez López, R., Lario Gómez, J., Perucha Atienza, M.A., Bardají Azcárate, T., Huerta Hurtado, P., Roquero García-Casal, E., Bautista Davila, M.B., 2014. Catálogo de los efectos geológicos de los terremotos en España. IGME y AEQUA, Madrid (352 pp.).

Silva, P.G., Goy, J.L., Somoza, L., Zazo, C., Bardají, T., 1993. Landscape response to strike-slip faulting linked to collisional settings: Quaternary tectonics and basin formation in the Eastern Betics, southeastern Spain. Tectonophysics 224 (4), 289–303. https://doi.org/10.1016/0040-1951(93)90034-H.

Silva, P.G., Goy, J.L., Zazo, C., Bardají, T., 2003. Fault-generated mountain fronts in southeast Spain: geomorphologic assessment of tectonic and seismic activity. Geomorphology 50, 203–225. https://doi.org/10.1016/S0169-555X(02)00215-5.

Snyder, N.P., Whipple, K.X., Tucker, G.E., Merritts, D.J., 2000. Landscape response to tectonic forcing: digital elevation model analysis of streamprofiles in the Mendocino triple junction region, northern California. GSA Bull. 112, 1250–1263. https://doi.org/10.1130/0016-7606(2000)112%3C1250:LRTTFD%3E2.0.CO;2.

Soria, F.J., López-Garrido, A.C., Vera, J.A., 1987. Análisis estratigráfico y sedimentológico de los depósitos neógeno-cuaternarios en el sector de Orce, depresión de Guadix-Baza. Paleontol. Evol. Mem. Esp. 1, 11–34.

Soria, J.M., Fernández, J., Viseras, C., 1999. Late Miocene stratigraphy and palaeogeographic evolution of the intramontane Guadix Basin (Central Betic Cordillera, Spain): implications for an Atlantic–Mediterranean connection. Palaeogeogr. Palaeoclimatol. Palaeoecol. 151 (4), 255–266. https://doi.org/10.1016/S0031-0182(99)00019-X.

Soria-Jáuregui, A., Jiménez-Cantizano, F., Antón, L., 2018. Geomorphic and tectonic implications of the endorheic to exorheic transition of the Ebro River system in Northeast Iberia. Quat. Res. 91 (2), 472–492. https://doi.org/10.1017/qua.2018.87.

Stokes, M., Mather, A., Rodés, Á., Kearsey, S., Lewin, S., 2018. Anatomy, age and origin of an intramontane top basin surface (Sorbas Basin, Betic Cordillera, SE Spain). Quaternary 1 (2). https://doi.org/10.3390/quat1020015 15 pp.

Sutherland, R., Norris, R.J., 1994. Late Quaternary displacement rate, paleoseismicity, and geomorphic evolution of the Alpine Fault: evidence from Hokuri Creek, South Westland, New Zealand. New Zealand J. Geol. Geophys. 38 (4), 419–430. https://doi.org/10.1080/00288306.1995.9514669.

Sylvester, A.G., 1988. Strike-slip faults. GSA Bull. 100, 1666–1703. https://doi.org/10.1130/0016-7606(1988)100%3C1666:SSF%3E2.3.CO;2.

Tchalenko, J.S., 1970. Similarities between shear zones of different magnitudes. Geol. Soc. Am. Bull. 81 (6), 1625–1640. https://doi.org/10.1130/0016-7606(1970)81[1625:SBSZOD]2.0.CO;2.

Ul-Hadi, S., Khan, S.D., Owen, L.A., Khan, A.S., 2013. Geomorphic response to an active transpressiveregime: a case study along the Chaman strike-slipfault, western Pakistan. Earth Surf. Process. Landforms 38, 250–264. https://doi.org/10.1002/esp.3272.

Valkanou, K., Karymbalis, E., Papanastassiou, D., Soldati, M., Chalkias, C., Gaki-Papanastassiou, K., 2020. Morphometric analysis for the assessment of relative tectonic activity in Evia Island, Greece. Geosciences 10 (7), 264. https://doi.org/10.3390/geosciences10070264.

Van der Wal, J.L.N., Nottebaum, V.C., Gailleton, B., Stauch, G., Weismüller, C., Batkhishig, O., Lehmkuhl, F., Reicherter, K., 2020. Morphotectonics of the northern Bogd fault and implications for Middle Pleistocene to modern uplift rates in southern Mongolia. Geomorphology 155, 107330. https://doi.org/10.1016/j.geomorph.2020.107330.

Vera, J.A., 1970a. Facies del Plioceno de la Depresión de Guadix-Baza. Cuad. Geol. Univ. Granada 1, 23–25.

Vera, J.A., 1970b. Estudio estratigráfico de la Depresión de Guadix-Baza. Bol. Inst. Geol. Miner. España 81, 429–462.

Vera, J.A., Fernández, J., López-Garrido, A.C., Rodríguez-Fernández, J., 1985. Geología y estratigrafía de los materiales plioceno-pleistocenos del sector Orce-Venta Micena (prov. Granada). Paleontol. Evol. 18, 3–12.

Vera, J.A., Rodriguez, J., Guerra, A., Viseras, C., 1994. La Cuenca de Guadix-Baza, Documents et Travaux de l' Institut géologique Albert de Lapparent. 14 pp. 1–17.

Viseras, C., 1991. Estratigrafía y sedimentología del relleno aluvial de la cuenca de Guadix (Cordilleras Béticas). (PhD Thesis)Universidad de Granada, Spain (344 pp.).

Walker, R.T., Bayasgalan, A., Carson, R., Hazlett, R., McCarthy, L., Mischler, J., Molor, E., Sarantsetseg, P., Smith, L., Tsogtbadrakh, B., Tsolmon, G., 2006. Geomorphology and structure of the Jid right-lateral strike-slip fault in the Mongolian Altay mountains. J. Struct. Geol. 28, 1607–1622. https://doi.org/10.1016/j.jsg.2006.04.007.

Wallace, R.E., 1968. Notes on stream channels offset by the San Andreas fault, Southern Coast Ranges, California. Proceedings of Conference on Geologic Problems of San Andreas Fault System. 11. Stanford Univ. Publ. Geol. Sci., pp. 6–21.

Whipple, K., 2004. Bedrock rivers and the geomorphology of active orogens. Annu. Rev. Earth Planet. Sci. 32, 151–185. https://doi.org/10.1146/annurev.earth.32.101802.120356.

Whipple, K., Tucker, G.E., 1999. Dynamics of the stream-power river incision model: Implications for height limits of mountain ranges, landscape response timescales, and research needs. J. Geophys. Res. Solid Earth 104, 17661–17674. https://doi.org/10.1029/1999JB900120.

Wobus, C.W., Whipple, K.X., Kirby, E., Snyder, N.P., Johnson, J., Spyropolou, K., Crosby, B.T., Sheehan, D., 2006. Tectonics from topography: procedures, promise and pitfalls. In: Willett, S.D., Hovius, N., Brandon, M.T., Fisher, D.M. (Eds.), Tectonics. Climate and Landscape Evolution: Geological Society of America, Special Paper398, pp. 55–74.

Yazici, M., Zabci, C., Sançar, T., Natalin, B.A., 2018. The role of intraplate strike-slip faults in shaping the surrounding morphology: the Ovacık Fault (eastern Turkey) as a case study. Geomorphology 321, 129–145. https://doi.org/10.1016/j.geomorph.2018.08.022.

Zhang, K., Liu, K., Yang, J., 2003. Asymmetrical valleys created by the geomorphic response of rivers to strike-slip fault. Quat. Res. 62 (3), 310–315. https://doi.org/10.1016/j.yqres.2004.07.003.

Zielke, O., Klinger, Y., Arrowsmith, J.R., 2015. Fault slip and earthquake recurrence along strike-slip faults — contributions of high-resolution geomorphic data. Tectonophysics 638, 43–62. https://doi.org/10.1016/j.tecto.2014.11.004.

Zuchiewicz, W., 1991. On different approaches to neotectonics: a polish Carpathians example. Episodes 14 (2), 116–124. https://doi.org/10.18814/epiiugs/1991/v14i2/002.

Zuchiewicz, W., 1998. Quaternary tectonics of the Outer West Carpathians, Poland. Tectonophysics 297, 121–132. https://doi.org/10.1016/S0040-1951(98)00226-1.